GEORGIA INSTITUTE OF TECHNOLOGY
Engineering Experiment Station

PROJECT INITIATION

Date: 3/21/72

Project Title: New Techniques and Indicators for Studies of Growth History of Zoned Crystals

Project No.: A-1409

Project Director: Dr. C. O. Pollard and Mr. C. E. Wagner

Sponsor: Army Research Office - Durham

Effective April 1, 1972 Estimated to run until: March 31, 1973

Type Agreement: Grant No. DA-ARO-D-31-124-72-G41 Amount: $ 24,869

Reports: Progress Reports; Final Technical Report.

Contact Persons:

Administrative
Mr. Jack L. Harless
Contracting Officer
Department of the Army
U. S. Army Research Office
Box CM, Duke Station
Durham, North Carolina 27706

Technical
Dr. Finn E. Bronner
Commanding Officer
U. S. Army Research Office
Box CM, Duke Station
Durham, North Carolina 27706

Project No. A-1409 is a follow-on to Project No. A-1306.

Assigned to Physical Sciences Division

COPIES TO:

- ☐ Project Director
- ☐ Director
- ☐ Associate Director
- ☐ Assistant Director(s)
- ☐ Division Chiefs
- ☐ Branch Head
- ☐ General Office Services
- ☐ Engineering Design Services
- ☐ Photographic Laboratory
- ☑ Research Security Officer
- ☐ Accounting
- ☐ Purchasing
- ☐ Report Section
- ☐ Library
- ☐ Rich Electronic Computer Center
- ☐ _____

EA-62(12-66)

GEORGIA INSTITUTE OF TECHNOLOGY
Engineering Experiment Station

PROJECT TERMINATION

Date December 6, 1973

PROJECT TITLE: New Techniques and Indicators for Studies of Growth History of Zoned Crystals

PROJECT NO: A-1409

PROJECT DIRECTOR: Dr. C. O. Pollard

SPONSOR: Army Research Office - Durham

TERMINATION EFFECTIVE: March 31, 1973

CHARGES SHOULD CLEAR ACCOUNTING BY: December 31, 1973

FINAL TECHNICAL REPORT: Completed

FISCAL REPORT

PHYSICAL SCIENCES DIVISION

COPIES TO:

Project Director
Director
Associate Director
Assistant Directors
Division Chief
Branch Head
Accounting
Engineering Design Services
General Office Services
Photographic Laboratory
Purchasing
Report Section
Library
Security
Rich Electronic Computer Center

EES 402 (R10–62)

PROGRESS REPORT No. 5

1. ARO-D PROPOSAL NUMBER: 8462 -EN

2. PERIOD COVERED BY REPORT: Ocotber 1, 1971 - March 31, 1972

3. TITLE OF PROPOSAL: New Technique and Indicators for Studies of Growth History of Zoned Crystals

4. CONTRACT OR GRANT NUMBER: DA-ARO-D-31-124-71-G64

5. NAME OF INSTITUTION: Georgia Institute of Technology

6. AUTHOR(S) OF REPORT: C. O. Pollard, Jr. and C. E. Wagner

7. LIST OF MANUSCRIPTS SUBMITTED OR PUBLISHED UNDER ARO-D SPONSORSHIP DURING THIS PERIOD, INCLUDING JOURNAL REFERENCES:

None

8. SCIENTIFIC PERSONNEL SUPPORTED BY THIS PROJECT AND DEGREES AWARDED DURING THIS REPORTING PERIOD:

C. O. Pollard, Jr.
C. E. Wagner
W. Scott Parks

CRDARD Form IP-129
16 Mar 67

Dr. C. O. Pollard
Mr. C. E. Wagner
Engineering Experiment Station
Georgia Tech Research Institute
Atlanta, Georgia 30332

8462-EN

R 6538

The microprobe results on R6538, a green sector-zoned tourmaline (which was described during September at the A.G.U. Conference on Petrologic Crystal Chemistry), need to be enhanced with more element determinations on a more close-spaced grid. Otherwise, it is difficult to relate our SID texture observations to the more common descriptions of crystal zoning by microprobe studies. Consequently, we have begun developing a series of standards and a computer data-reduction program to obtain better probe data on this and other crystals.

The new texture, described from R-6538 in Progress Report No. 4, involving misorientations by rotation about c-axis directions, turns out to be rare and to be restricted to small portions of the crystal; therefore, it seems to be difficult to characterize (yet, it is essentially as described in Report No.4).

Staurolite

Overgrowth lamellae, superficially like those originally described by us in growth-zoned tourmaline but not yet well characterized, have been found by using XRD Lang topography in one of two sector-zoned Kwioek (British Columbia) staurolite crystals which were originally studied with the microprobe by Lincoln Hollister and Wayne Dollase. Larger scale misorientations that are not attributable to cracks are also present, in the core.

Andalusite

The domains of misorientation (approx. 1°, by rotations about a c-axis direction) previously predicted by Hafner, Raymond, and Ghose [J. Chem. Phys. 52, 6037 (1970)] in an andalusite crystal have now been sought on an internal slice and still have not been found. Some SID-textural infermation has been obtained, but so far no misorientations have been observed as large as $\frac{1}{4}^{\circ}$.

Origin of SID texture

AT-cut quartz blanks have been mapped by SID for pre-existing texture, placed in torsion ($> \frac{1}{2}$ fracture load) at $> 600^{\circ}C$, and then remapped by SID. Several improvements have been made in surface preparation of the blanks and in temperature control, but reproducibility is still a problem. We are improving the temperature profile of the oven and are obtaining before and after Lang topographs as well.

A-1409

PROGRESS REPORT No. 6

1. ARO-D PROPOSAL NUMBER: 8462-EN

2. PERIOD COVERED BY REPORT: 1 April 1972 - 30 September 1972

3. TITLE OF PROPOSAL: New Technique and Indicators for Studies of Growth History of Zoned Crystals.

4. CONTRACT OR GRANT NUMBER: DA - ARO - D - 31 - 124 - 72 - G41

5. NAME OF INSTITUTION: Georgia Institute of Technology

6. AUTHOR(S) OF REPORT: C. O. Pollard, Jr.

7. LIST OF MANUSCRIPTS SUBMITTED OR PUBLISHED UNDER ARO-D SPONSORSHIP DURING THIS PERIOD, INCLUDING JOURNAL REFERENCES:

None.

8. SCIENTIFIC PERSONNEL SUPPORTED BY THIS PROJECT AND DEGREES AWARDED DURING THIS REPORTING PERIOD:

C. O. Pollard, Jr.
C. E. Wagner
W. Scott Parks

Dr. C. O. Pollard
Mr. C. E. Wagner
Engineering Experiment Station
Georgia Tech Research Institute
Atlanta, Georgia 30332

BRIEF OUTLINE OF RESEARCH FINDINGS

R-6538

The microprobe results for R-6538 have been obtained. Within each of the two types of sector zones (light green and dark green), no compositional variation was detected.

The microprobe analysis is summarized in the following table (components in weight percentages):

	SiO_2	Al_2O_3	FeO (total Fe)	Na_2O	MnO (total Mn)
Light green sectors:	35.36±0.19	41.08±0.20	5.95±0.12	2.90±0.06	1.09±0.04
Dark green sectors:	34.64±0.19	41.62±0.20	5.99±0.12	2.92±0.06	1.12±0.04

	CaO	MgO	TiO_2 (total Ti)	K_2O
Light green sectors:	0.17±0.01	0.11±0.01	0.07±0.02	0.04±0.01
Dark green sectors:	0.16±0.01	0.11±0.01	0.11±0.02	0.05±0.01

The SiO_2 and Al_2O_3 differences are the only ones that exceed significantly the counting-rate errors. It is obviously not possible to attribute the difference in color intensity positively to differences in percentages of any of the transition elements.

Polarized ultraviolet-visible transmission spectra were obtained for the two types of sectors, to aid in explaining the color differences. The 14,000 cm^{-1} and 24,000 cm^{-1} absorption peaks that have been reported in earlier literature were found. The E$\|$c and E$\perp$c spectra looked similar to those in Figure 3 of Faye et al [Amer. Min., 53, 1174 (1968)], but with a definite broad peak centered at 24,000 cm^{-1}. It was impossible to obtain E$\|$c spectra from the separate sectors, but E$\perp$c spectra from both types of sectors were obtained. The E$\perp$c spectra of the dark green sectors were similar to the E$\perp$c spectra of the light green sectors, but the absorbance was approximately 10% greater at each wavelength in the dark sectors. Such spectral behavior supports one of three interpretations: (1.) the two absorbing species (corresponding to bands at 14,000 cm^{-1} and 24,000cm^{-1}) are diluted similarly in the light green sectors relative to the dark green sectors, (2.) a single ion is responsible for both absorptions (such as an electronic transition and a charge transfer, both involving Fe^{2+}), and (3.) a coupled diadochous substitution increases the absorbing species responsible for each band simultaneously (such as $Fe^{3+}+Ti^{4+} \rightleftarrows Ti^{3+}+Si^{4+}$). Faye et al attribute the 14,000 cm^{-1} band to charge transfer involving Fe^{2+} and Fe^{3+} ions in neighboring sites, which are equivalent to each other by the trigonal symmetry. They attribute the 24,000 cm^{-1} band to a similar Ti^{3+}-Ti^{4+} charge transfer mechanism. Assuming their assignments are correct, mechanism (2.) above is not possible, however, our probe and spectral data do not allow an unambiguous choice between mechanisms (1.) and (3.). We intend to obtain the missing E$\|$c spectra for each type of sector, which may allow distinction between mechanisms (1.) and (3.).

The manuscript dealing with R-6538 is being revised to account for these new findings.

BRIEF OUTLINE OF RESEARCH FINDINGS

AT - Cut Quartz

There are two possible orientations of the AT - cut blanks in the torsion apparatus. They are not symmetrically equivalent. The appropriate orientation is recorded for each blank that is mapped, heated to above 600°C under torsion, and remapped. The before mapping consists of multi-source SID and Lang topography with 210, 012, and 301 reflections. We have found that the crystals must be reetched after heating to remove surface damage that is created during heating. The crystals are then remapped by SID and Lang topography using the same three reflections. The crystals usually break nearly along a diagonal during heating, even though the round trip from room temperature takes longer than 24 hours, with particularly slow-temperature changes within 20°C of the α-β conversion point. The data from a broken crystal are used only if the fracture cuts across the other created features. So far, no device has allowed positive indication of the time of fracturing of broken crystals.

The features that are most frequently created during heating are Dauphiné twins. The twin composition surfaces seem to prefer to coincide with preexisting growth horizon boundaries, but locally the two surfaces diverge. When the twin composition surfaces are not coincident with growth horizons, the composition surfaces are more irregular in trend and usually are non-cylindrical. Pendellösung fringes are evident, along with oblique linear features that are not Pendellösung fringes. Too few of these linear features have been observed to be characterized. Possibly they correspond to the steps noted on naturally-produced Dauphiné twin boundaries by Lang [Crystal Growth, Suppl. to The Journal of Physics and Chemistry of Solids, Proceedings of an International Conference, Boston, 20-24, June 1966, pp. 833-838].

It is to correlate created features (such as these linear features in twin boundaries) with natural features that the heating experiments are being conducted.

Personnel

Mr. Derrold Holcomb has been hired as a student assistant, to help with the dark-room and SID work.

NEW TECHNIQUE AND INDICATOR FOR STUDIES OF GROWTH HISTORY OF ZONED CRYSTALS

Progress Report

C. O. Pollard, Jr.
2 May 1973

U. S. Army Research Office - Durham

DA-ARO-D-31-124-72-G41

Georgia Institute of Technology

THE FINDINGS IN THIS REPORT ARE NOT TO BE CONSTRUED AS AN OFFICIAL DEPARTMENT OF THE ARMY POSITION, UNLESS SO DESIGNATED BY OTHER AUTHORIZED DOCUMENTS.

Unclassified

Security Classification

DOCUMENT CONTROL DATA - R & L

(Security classification of title, body of abstract and indexing annotation must be entered when the overall report is classified)

1. ORIGINATING ACTIVITY *(Corporate author)*

Georgia Tech Research Institute
Georgia Institute of Technology
Atlanta, Georgia 30332

2a. REPORT SECURITY CLASSIFICATION

Unclassified

2b. GROUP

NA

3. REPORT TITLE

New Technique and Indicators for Studies of Growth History of Zoned Crystals

4. DESCRIPTIVE NOTES *(Type of report and inclusive dates)*

Progress Report

5. AUTHOR(S) *(First name, middle initial, last name)*

Charles O. Pollard, Jr.

6. REPORT DATE	7a. TOTAL NO. OF PAGES	7b. NO. OF REFS
2 May 1973	2	1

8a. CONTRACT OR GRANT NO.	9a. ORIGINATOR'S REPORT NUMBER(S)
DA-ARO-D-31-124-73-G41	
b. PROJECT NO.	
Proposal No. 8462EN	No. 7
c.	9b. OTHER REPORT NO(S) *(Any other numbers that may be assigned this report)*
d.	

10. DISTRIBUTION STATEMENT

Approved for public release; distribution unlimited

11. SUPPLEMENTARY NOTES	12. SPONSORING MILITARY ACTIVITY
	U. S. Army Research Office - Durham Box CM, Duke Station Durham, North Carolina 27706

13. ABSTRACT

The sector-zoned tourmaline (elbaite) crystal - Smithsonian R6538 - apparently has fine chemical domains on a scale of 40-100 μm, as revealed by microprobe Si-Kα scans, within at least the light green sectors.

AT-cut quartz crystals can be made to Dauphine twin by torsion at above 600°C, such that the twin boundaries assume veil-like shapes with steps, except where they correspond to pre-existing growth horizon boundaries. Strain rate controls and recording are needed to exclude problems with fracturing.

Andalusite contains misorientation domains involving rotations of 1° to 2° about an axis normal to [001].

DD FORM 1 NOV 1473 REPLACES DD FORM 1473, 1 JAN 64, WHICH IS OBSOLETE FOR ARMY USE.

Unclassified

Security Classification

14. KEY WORDS	LINK A		LINK B		LINK C	
	ROLE	WT	ROLE	WT	ROLE	WT
Tourmaline, quartz, adnalusite, AT-cut quartz, chemical domains, misorientation domains, Dauphiné twinning.						

PROGRESS REPORT NO. 7

1. ARO-D PROPOSAL NUMBER: 8462-EN

2. PERIOD COVERED BY REPORT: 1 October 1972 - 31 March 1973

3. TITLE OF PROPOSAL: New Technique and Indicator for Studies of Growth History of Zoned Crystals

4. CONTRACT OR GRANT NUMBER: DA-ARO-D-31-124-72-G41

5. NAME OF INSTITUTION: Georgia Institute of Technology

6. AUTHOR(S) OF REPORT: C. O. Pollard, Jr.

7. LIST OF MANUSCRIPTS SUBMITTED OR PUBLISHED UNDER ARO-D SPONSORSHIP DURING THIS PERIOD, INCLUDING JOURNAL REFERENCES:

C. O. Pollard, Jr. and C. E. Wagner (1973) "Strains Associated with Chemical Boundaries in a Sector-Zoned Elbaite Tourmaline Crystal" (Abstract) Geol. Soc. Amer., S.E. Section Annual Meeting

8. SCIENTIFIC PERSONNEL SUPPORTED BY THIS PROJECT AND DEGREES AWARDED DURING THIS REPORTING PERIOD:

C. O. Pollard, Jr.

W. Scott Parks

Derrold Holcomb

Dr. C. O. Pollard
Engineering Experiment Station
Georgia Tech Research Institute
Atlanta, Georgia 30332

PROGRESS REPORT NO. 7

BRIEF OUTLINE OF RESEARCH FINDINGS

R6538 - Smithsonian tourmaline crystal

Compositional microprobe variations within each of the two (light green and dark green) types of sectors have apparently been detected. The data must be reproduced, but SiO_2 apparently varies as much as five times more than the instrumental fluctuations over a linear distance of 40-100 μm. In order to detect this variation, it was necessary to scan an electron beam with spot size of 10 μm at a scan rate of 80 μm/minute. The next step is to determine whether these variations are real or artifacts (say, because of surface roughness). One implication of the variations is that the microprobe results reported in Progress Report No. 6 should be interpreted as average analyses with the variations yet to be determined.

New Lang topographs have been obtained which show a fine-scale lamellar feature in one portion of a light-green sector, the lamellar thickness averaging 30-50 μm. The lamellae may be compositional domains that correspond to the SiO_2 variations described in the first paragraph, but their apparent restriction to the small area of the section is puzzling. Obviously, the data for R6538 need reinterpreting when they have been rechecked.

The differences in the color of the two types of sectors are still not explained, if the composition is as nearly the same as has been found (particularly in view of the new evidence that the composition varies spatially within each sector). R. G. Burns (personal communication) has found no evidence for Fe^{3+} in green tourmaline by Mössbauer spectroscopy. (He now has a portion of R6538 and intends to obtain spectra from the light green and dark green sectors.) His interpretation of Mössbauer spectra from other green tourmalines is that Fe^{2+} occupies both the 6-coordinated sites and that the assignment by Faye, et al. (1968) of the 14,000 cm^{-1} UV-Vis absorption peak was in error. He thinks that peak is more likely a Fe^{2+} crystal-field band and advances no explanation for the 24,000 cm^{-1} UV-Vis absorption peak.

AT-Cut Quartz

The Dauphiné twin boundaries that have been created assume a veil-like shape in the regions where they do not correspond to pre-existing growth horizons. If we expect to prove that some of the created features correspond to features in natural quartz that has passed through the α-β transition under torsion, it is imperative that we be able to control the strain rate better than we are doing with the passive loading we are now using. In addition, we need to be able to determine when fracture occurs in the temperature cycle if it occurs; otherwise, the observations from many fractured samples must be discarded when it cannot be demonstrated from the topographs that fracture boundaries post date all other boundaries.

Andalusite

Domains of misorientation have been found in andalusite by the Schultz (Laue transmission) topographic technique. The magnitude of misorientations (about 1° or 2° of arc) matches that reported from NMR data by Hafner, et. al., but the axis of rotation seems to be normal to [001], rather than parallel to it. We will recheck our data and have them recheck theirs.

Bibliography

Faye, et al., Amer. Min., 53, 1174 (1968).

Hafner, et al., J. Chem. Phys., 52, 6037 (1970).

NEW TECHNIQUE AND INDICATOR FOR STUDIES OF GROWTH HISTORY OF ZONED CRYSTALS

Final Report

Report No. 8

C. O. Pollard, Jr.

31 August 1973

U. S. Army Research Office - Durham

Contract No. DAHC04-70-C-0012
Grant No. DA-ARO-D-31-124-71-G64
Grant No. DA-ARO-D-31-124-72-G41

Georgia Institute of Technology

Project No. A1217
Project No. A1306
Project No. A1409

THE FINDINGS IN THIS REPORT ARE NOT TO BE CONSTRUED AS AN OFFICIAL DEPARTMENT OF THE ARMY POSITION, UNLESS SO DESIGNATED BY OTHER AUTHORIZED DOCUMENTS.

Unclassified
Security Classification

DOCUMENT CONTROL DATA - R & D

(Security classification of title, body of abstract and indexing annotation must be entered when the overall report is classified)

1. ORIGINATING ACTIVITY *(Corporate author)*
Georgia Tech Research Institute
Georgia Institute of Technology
Atlanta, GA 30332

2a. REPORT SECURITY CLASSIFICATION
Unclassified

2b. GROUP
NA

3. REPORT TITLE
New Technique and Indicators for Studies of Growth History of Zoned Crystals

4. DESCRIPTIVE NOTES *(Type of report and inclusive dates)*
Final Report for period 1 November 1969 to 30 September 1973

5. AUTHOR(S) *(First name, middle initial, last name)*
Charles O. Pollard, Jr.

6. REPORT DATE
31 August 1973

7a. TOTAL NO. OF PAGES
68 w/reprint as App. I, 86 w/preprint.

7b. NO. OF REFS
24

8a. CONTRACT OR GRANT NO.
Grant DA-ARO-D-31-124-71-G64
Grant DA-ARO-D-31-124-72-G41

b. PROJECT NO.
Contract No. DAHC04-70-C-0012
Proposal No. 8462EN

c.

d.

9a. ORIGINATOR'S REPORT NUMBER(S)
No. A1409-8

9b. OTHER REPORT NO(S) *(Any other numbers that may be assigned this report)*

10. DISTRIBUTION STATEMENT
Approved for public release; distribution unlimited

11. SUPPLEMENTARY NOTES

12. SPONSORING MILITARY ACTIVITY
U.S. Army Research Office - Durham
Box CM, Duke Station
Durham, N. C. 27706

13. ABSTRACT

Two X-ray diffraction imaging techniques have been applied for the first time to the study of previously unnoted mosaic detail in color-zoned Brazilian tourmaline. The divergence source-image distortion (DSID) technique gives maximum values for misorientations among all observable grains, whereas the convergence source-image distortion (CSID) technique yields the magnitude of misorientation between adjacent grains. Strikingly abrupt textural changes are observed; they are always accompanied by color changes. The converse is not found to hold. The central or core region of all five plates studied shows a macromosaic texture corresponding to an intrinsic rocking curbe that would have a width at half height of ~1.2 minutes of arc. No grain elongation is observed. U

The core region is sharply delineated from a surrounding ring or overgrowth region of lamellar texture, in which grains approximate $(2\bar{1}\bar{1}0)$ lamellae. The lattices of the lamellae in a given region are tilted with respect to each other by angles predominantly less than 5 minutes of arc but ranging up to 13 minutes of arc, the tilt axis being parallel to the long dimension of the lamella in the basal plane. The lamellar grains are subparallel in a given boundary region, and are normal to the growth boundaries on the $(01\bar{1}0)$, $(\bar{1}010)$ $(\bar{1}100)$ faces but on the other three regions they are parallel to the lamellae on an adjacent boundary. Electron microprobe traces rule out exsolution and compositional domain structures as an explanation of lamellar texture. Sudden drastic changes in conditions controlling crystal growth are possible causes of our observations. U

AT-cut quartz crystals can be made to Dauphine twin by torsion at above 600°C, such that the twin boundaries assume veil-like shapes with steps, except where they (con't)

DD FORM 1 NOV 65 1473 REPLACES DD FORM 1473, 1 JAN 64, WHICH IS OBSOLETE FOR ARMY USE.

Unclassified
Security Classification

14. KEY WORDS	LINK A		LINK B		LINK C	
	ROLE	WT	ROLE	WT	ROLE	WT
X-ray diffraction topography, source-image distortion, tourmaline, quartz, andalusite, topaz, AT-cut quartz, twinning domains, misorientation domains, Dauphiné twinning, pyrite, europium aluminum garnet, trigylcine sulfate, sphalerite, schorl, apatite, corundum, sapphire, garnet, staurolite, fluorite, calcite						

correspond to pre-existing growth horizon boundaries. Strain rate controls and recording are needed to exclude problems with fracturing. U

The color zones of the elbaite crystal R6538 (Smithsonian) lie in a sectorial pattern; however, microprobe and visible-light spectrophotometric results indicate that the two types of sectors are essentially the same chemically (with the slightly possible exception of Al_2O_3 and SiO_2). Basal plates of the crystal are light green in the first-order prism sectors and dark green in the second-order prism sectors. No measurable cell-parameter differences across sector boundaries have been detected. Rotational misorientations are measurable at some of the sector boundaries, each involving a rotation of less than 40 seconds of arc around an axis parallel to the boundary normal. These rotational misorientations can be measured on boundaries that are roughly parallel to second-order prism faces, separating sectors behind first and second-order prism faces. The basal component of the fault vector characteristic of any particular sector boundary is observed to lie normal to the boundary for all the fault vectors whose orientations could be determined. Only one boundary (roughly parallel to a first-order prism face and separating sectors behind first and second-order prism faces) was describable purely by a fault vector, with no rotational misorientation. U

Striae are found within the sectors (in x-ray diffraction SID patterns and Lang topographs) that indicate that the optical sectoring of R6538 is due to different scattering interactions between light and domains of different shapes in the two types of sectors. The domains are apparently linear or cylindrical in the dark green sectors and lamellar in the light green sectors. Those in the dark green sectors are apparently elongated roughly along the c-axis direction and those in the light-green sectors are apparently oriented so that the c-axis direction lies roughly in the lamellae. These domains may correspond to the twinning domains recently proposed by Tsang and Ghose [1973]. U

Abrupt textural changes have been found in SID patterns from two crystals of topaz - $Al_2SiO_4(OH,F)_2$. The textural boundaries correspond to boundaries under the polarizing microscope between undulatory and sharply extinguishing portions. Needle-like inclusions (apparently, but not certainly, TiO_2) are found only in the rims of these crystals. U

Many other crystals were examined by SID and Lang topographic techniques and found to be featureless or (more commonly) to be too imperfect. U

TABLE OF CONTENTS

LIST OF APPENDICES

I. Reprint (some bindings contain preprints instead) of resulting article entitled "Texture Variations in Color-Zoned Tourmaline Crystals"

II. Reference to an oral presentation, reference to an abstract, and a copy of a resulting manuscript entitled "Strains Associated with Color Boundaries in a Sector-Zoned Tourmaline (Elbaite) Crystal"

LIST OF ILLUSTRATIONS

Fifteen illustrations are found in the article in Appendix I.

Four illustrations are found in the manuscript in Appendix II.

Two illustrations appear in the body of the report, as follows:

PARTICIPATING SCIENTIFIC PERSONNEL

C.O. Pollard, Jr., Co-Principal Investigator

C.E. Wagner, Co-Principal Investigator until 29 September 1972

W. Scott Parks, Jr., Graduate Research Assistant

J. Conrad Meadors, Assistant Research Engineer

R. A.Young, Professor of Physics

Derrold Holcomb, Technical Assistant

James R. Cagle, Assistant Research Scientist

James W. Johnson, Research Scientist

LIST OF RESULTING PUBLICATIONS

Young, R. A., C. E. Wagner, C. O. Pollard, and G. Donnay (1969) Evidence from source-image distortion, Annual Report of the Director, Geophysical Laboratory, Carnegie Institute Year Book 67, pp. 220-221.

Wagner, C. E., C. O. Pollard, Jr., R. A. Young, and Gabrielle Donnay (1971) Texture variations in color-zoned tourmaline crystals, Amer. Mineral. 56, pp. 114-132. (See Appendix I.)

Pollard, C. O., Jr., and C. E. Wagner (1971) X-ray diffraction topographic and source-image distortion study of sector zoning in a tourmaline crystal (oral), Amer. Geophys. Union. Conference on Petrologic Crystal Chemistry. (See Appendix II.)

Pollard, C. O., Jr., and C. E. Wagner (1973) Strains associated with chemical boundaries in a sector-zoned elbaite tourmaline crystal (Abstract), Geol. Soc. Amer., S. E. Section Annual Meeting in Knoxville. (See Appendix II).

Pollard, C. O., Jr., and W. S. Parks, Jr. (1973) Strains associated with color boundaries in a sector-zoned tourmaline (elbaite) crystal (To be submitted - See Appendix II.)

CONTRACT AND GRANT NUMBERS

Contract No. DAHC04-70-C-0012

Grant No. DA-ARO-D-31-124-71-G64

Grant No. DA-ARO-D-31-124-72-G41

PROBLEMS STUDIED

Characterization of Natural Features

The principal efforts of the project were invested in searches for features in minerals that could best be characterized by the x-ray diffraction topographic techniques and source-image distortion (SID) techniques. It was recognized all along that many crystals would not be suited, usually because of concentrations of imperfections that were too high; however, the rewards of the previously uncharacterizable features in the small percentage of appropriate crystals made the inefficient searching process worth the effort. When suitable crystals were found, some of the searching effort was diverted to conduct as complete an effort as considered appropriate to fully characterize the nature of the discovered topographic and SID features. This full characterization is in different stages of completion for different materials.

Negative results. Those materials (some artificial, but most natural) that were searched and found void of usable textural information (either featureless or too densely populated with imperfections) after a reasonable investment of search time are as follows: pyrite (deformed and undeformed), europian aluminum garnet (artificial), triglycine sulfate (artificial), sphalerite (both artificial and natural), schorl tourmaline, quartz (many crystals were useful, but many more were not), apatite, andalusite (although some information could be obtained, it was not fully characterizable), corundum (overgrown sapphire on clear corundum), natural garnet, staurolite, fluorite, and optical calcite. The presence of a mineral species in this list is not proof that it could not profitably be studied by topographic or SID techniques; rather it means that we were forced by considerations of efficiency to conclude that we should abandon the search with the samples we had collected. It is noteworthy that most of these samples were selected because we thought them to be the most promising on the basis of the knowledge at the time.

Positive results. A much smaller group of crystals contained textural features that we deemed appropriate for fuller characterization, with an aim toward producing a manuscript for publication in the refereed literature. One such report has been published (See Appendix I) on the textural features developed in several overgrown tourmaline crystals. Another manuscript is written and is virtually ready (awaiting criticism by a reader) to be submitted (See Appendix II); the subjects of this article are the different textural features found in a tourmaline crystal with sectorial color zones and the physical property changes that related to the textural features. Aspects of the findings were also reported orally and in an abstract (See Appendix II). Another group of crystals in which we have found features that are apparently appropriate for full study by topographic and SID techniques are a collection of topaz crystals with both overgrowth and sector zoning. The features in the topaz crystals have been only poorly characterized and the study is not near the manuscript stage. Another study in which "positive" results of a sort were obtained involves andalusite. In the andalusite study, a specific question was to be answered; luckily, the topographs obtained, although of a poorer quality than those obtained in any other "positive" study, allowed us to determine whether or not orientational domains existed in the andalusite as proposed by Hafner, Raymond and Ghose (1970).

Creation of Texture in Quartz

A series of before-and-after experiments were run to attempt to create inperfections in quartz crystals, for possible correlation with natural imperfections. If such features could be correlated in amenable ubiquitious minerals, fine zonation may be possible in studies of metamorphic rank or of strain facies.

The crystals selected for study are a series of AT-cut quartz oscillator plate blanks that are approximately 2.5cm x 2.5cm x 0.5mm in shape. The blanks

have previously been finished about to the equivalent of a 10 micron grit grinding compound. In order to determine if a particular crystal is suitably devoid of imperfections, mapping is done by the transmission multislit SID technique using the $0\bar{1}2$, the $2\bar{1}0$, and the 301 reflections. Such undesirable imperfections as growth horizons, inclusions, high concentrations of dislocations, and twins can be discerned in these patterns, even though there is a lot of clutter in the patterns due to surface strain. Once a crystal is selected as a candidate for the before-and-after experiments, the blank must be polished and then etched or it must be etched for a longer period of time; either way requires about four hours of preparation time so that the crystal can be mapped by topography. The crystals are then mapped by transmission Lang topography using the same three reflections, to complete the before portion of the experiment.

The stress portion of the experiment involves establishing an artificial state of strain in the crystal while temperature is elevated to the range in which plastic deformation is known to begin. For the experiments conducted to date, the temperature has been cycled through 600°C and back to room temperature on a 24-hour schedule with a slower heating rate within 10°C of 573°C. The crystal-stressing apparatus has been of two kinds. First, a simple bending device with three knife-edges was used. Second, a torsion frame with four force application points was used. Both were designed after apparatus suggested by Thomas and Wooster (1951) for stressing quartz. Neither one is adequate to produce good enough control on the state of strain established in the crystal for final experiments to be conducted; however, the torsion apparatus has worked well enough to demonstrate that better equipment would produce useful information. The principal problems with both types of apparatus are the variable (and unknown) friction effects and the lack of control on the strain rate. The bending apparatus inherently has more frictional loss than the torsion apparatus and was abandoned for that reason.

The "after" experiments involve obtaining a set of three topographs using

the same reflections. Recently the after topographs were observed to be of consistently lower quality than the before topographs, and the cause was found to be new surface strain that contributed background clutter throughout the topographs. Consequently, "after" topographs are now obtained when the induced surface strain is removed by etching for about two hours.

RESULTS AND CONCLUSIONS REACHED

In accordance with the directions for writing Final Reports from ARO-D, no technical findings will be reported that have already been reported in the Semi-Annual Progress Reports. Moreover, the findings and conclusions reported in the manuscripts that have been completed will not be repeated in this section (See Appendices I and II). General findings will be emphasized.

SID and topographic techniques are applicable to the study of many of the materials-science aspects of mineral crystals. There are restrictions on the application of these techniques and they must be supplemented by other techniques frequently, but there are a group of important features that can not be studied by other means. The first restriction on their application is that the crystals must be suitable. It is a necessary, but not sufficient, condition that the crystal be nearly perfect, as the sample may be essentially featureless or it may have uniform uncharacterizable clutter in its patterns. At this stage in the development of the application of SID and topographic techniques to mineralogic studies, the monotonous crystals probably are not suitable. The other extreme of suitability is those much more numerous crystals that have "too much" information in their patterns. These are the crystals that do not allow correlation of features on a one-for-one basis between sample and image because several features are imaged at or nearly at the same place and can not be resolved. Most of the suitable crystals we have found to date could best be labeled "gemmy." The high quality required of the samples that are suitable limits the application of these techniques for natural samples; nevertheless,

they are applicable to many growth-history, strain-mechnism, and temperature-response studies. As we have learned from examining many promising crystal species that did not turn out to be suitable, visual screening excludes only the most obvious candidates. Topographs and SID patterns must actually be obtained to determine the real suitability of a crystal species.

Many of the samples we have attempted to study by topography and SID techniques might have been better suited for transmission electron microscopy (TEM). There is a nebulous boundary in terms of density of imperfections that corresponds to the maximum density that is optimum for topography and to the minimum density that is optimum for TEM. An indicated future experiment is to try to image (by TEM) the Tsang-Ghose domains suspected in the R6538 tourmaline crystal (Appendix II).

The most promising mineral species bearing topographic features that have not been fully characterized is a group of zoned topaz crystals. The topographs from these crystals reveal bundles of dislocations, overgrowth zones, sector boundaries (if not sector zones), and strain fields around visible acicular inclusions. The bundles of dislocations are radially disposed and change character as they cross overgrowth boundaries. Burgers vectors associated with the dislocations retain the same orientation as the bundles cross overgrowth boundaries. A transmission $(2\bar{2}0)$ Lang topograph of one of the topaz crystals is shown in Figure A.

The before-and-after experiments on AT-cut quartz have shown that the method proposed in 1951 by Thomas and Wooster, for clearing twinned regions from potential oscillator plates of quartz, is not infallible. The success of the method, which requires heating and then cooling the crystal slowly through the α-β transition temperature while it is understress, apparently depends strongly on crystal orientation and sample shape. In fact, we have found that for the two possible orientations of the AT-cut blanks in the torsion frame, Dauphiné twins are created (instead of destroyed) by the experiment and details of

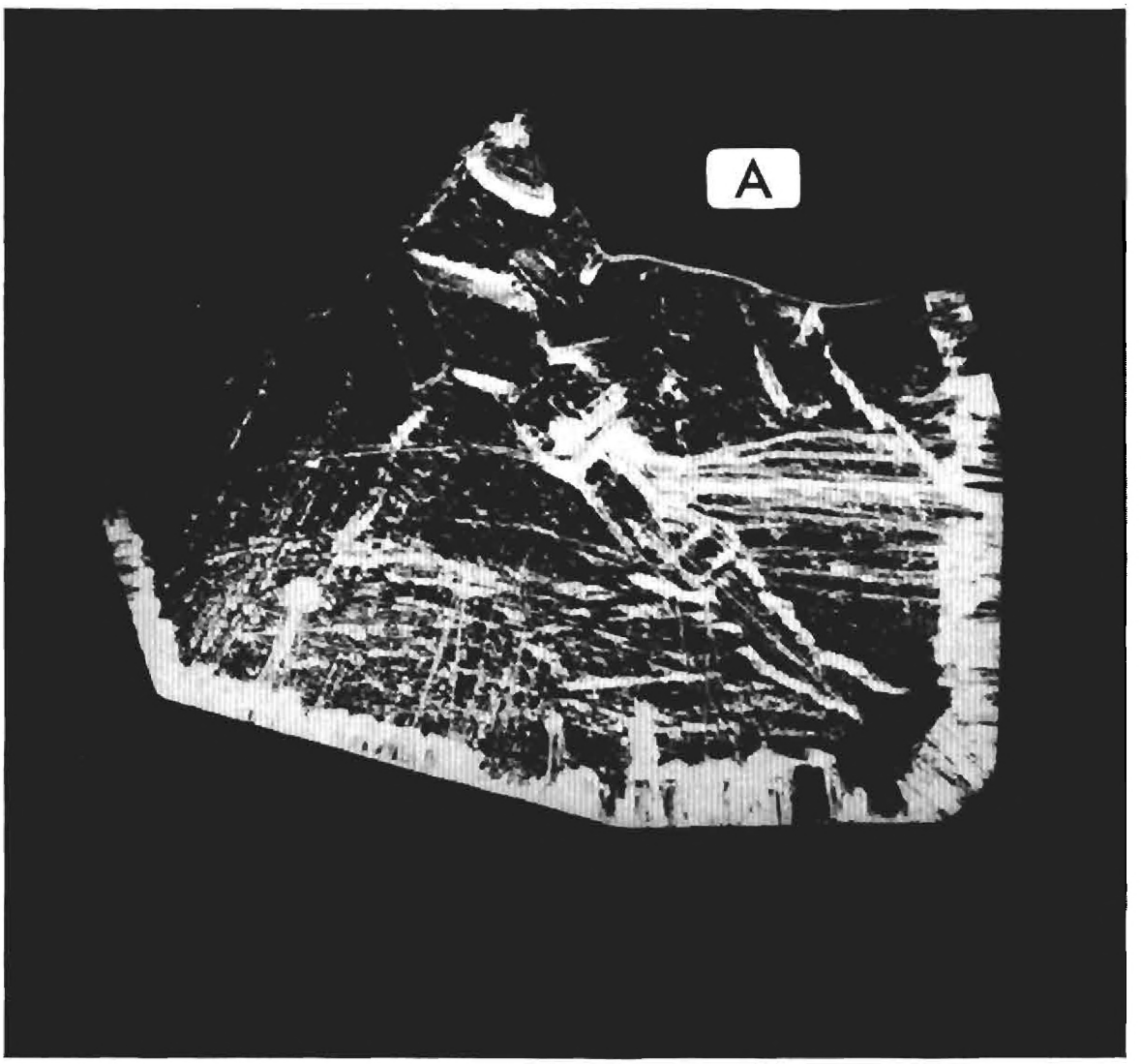
A

Dauphiné twin boundaries can be depicted readily in "after" topographs. The twin boundaries show an inclination to develop so that they coincide with pre-existing growth horizons that are commonly apparent in the "before" topographs. When the twin boundaries diverge from the straighter growth boundary segments, they assume veil-like aspects. Step-like features at Dauphiné twin boundaries are the only features we have created that we recognize from topographs of natural quartz crystals. Such steps were reported in natural crystals by Lang (1967). Figure B1 and B2 show ($0\bar{1}.2$) Lang topographs before and after the torsion experiment on a typical AT-cut quartz crystal. To delimit the conditions for development of these features will require better design of the stressing apparatus (control of strain rate, less friction). The redesigned equipment and development of adequate control on the experiments will be a large enough effort to justify a proposal for additional funds.

Other results and conclusions can be found in the manuscripts in Appendices I and II.

SUGGESTED FUTURE STUDIES

Several of the features we have discovered in tourmaline, quartz, and topaz involve densities of imperfections that are nearly too high to be characterized appropriately by topography and SID techniques. For instance, all the evidence from the sector-zoned tourmaline R6538 suggests there are linear domains of nearly micron size that are differently oriented in the light green and the dark green sectors (Appendix II). Other, coarser linear features of the correct orientations are resolvable with the appropriate topographic images; however, the suspected features are below the level of resolution of topography, particularly with the additional features crowding the patterns. Transmission electron microscopy (TEM) is indicated as the appropriate technique to use with such high densities of imperfections. R6538-5, a basal plate from the same tourmaline crystal should be thinned by ion bombardment (not available at Georgia

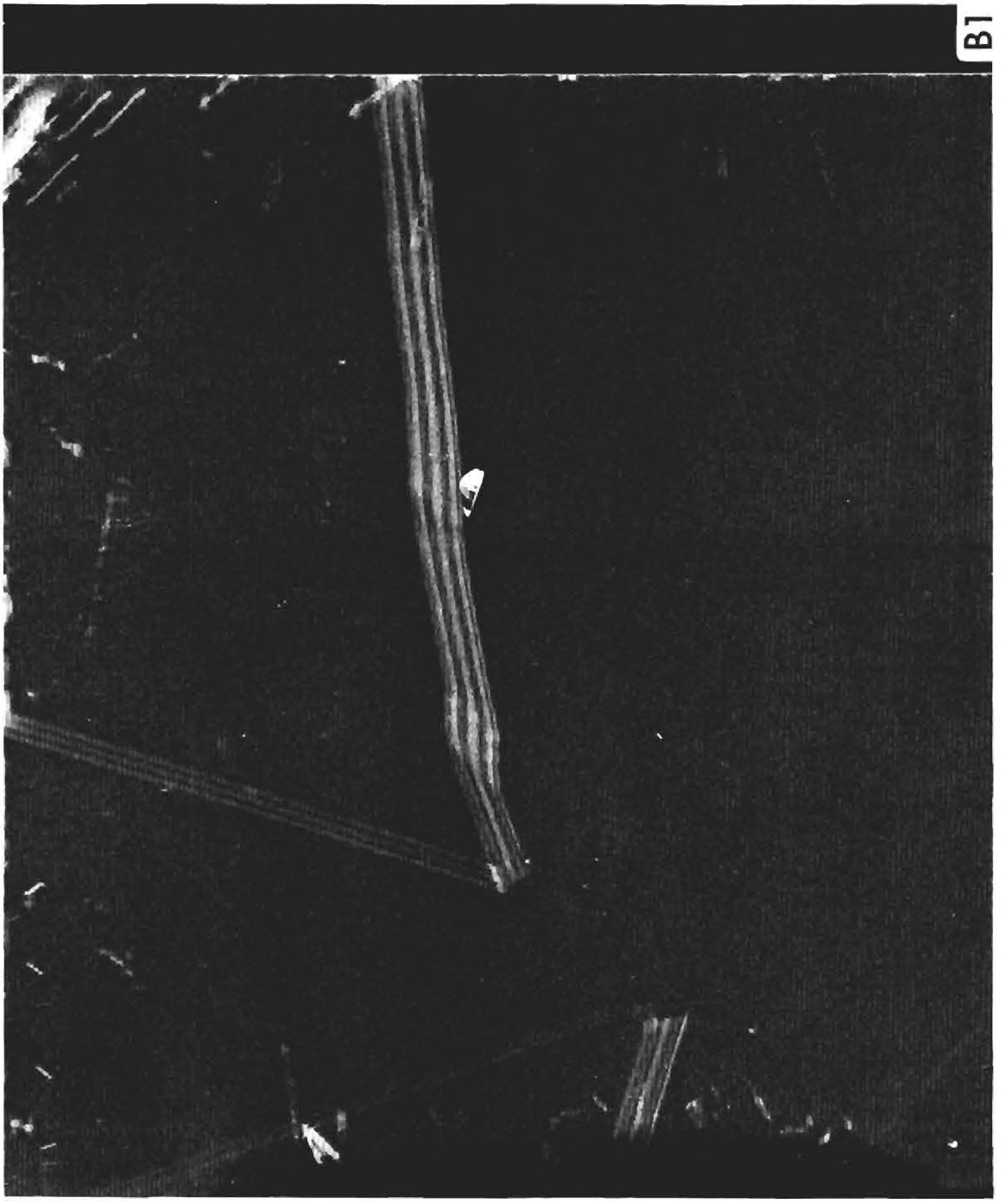
B1

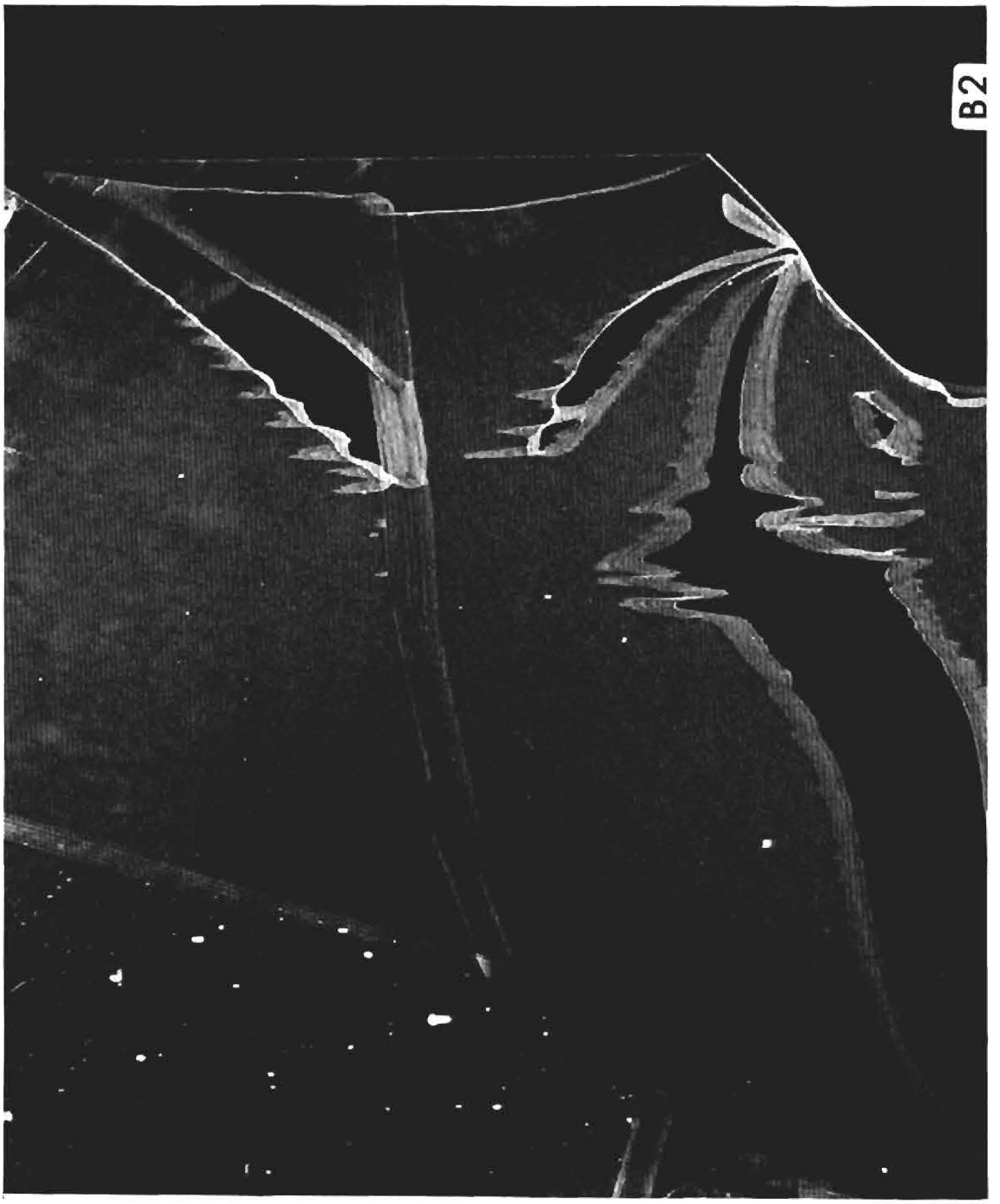
B2

Tech) and searched for the proposed features, which may correspond to the twinning domains recently suggested for elbaite by Tsang and Ghose (1973). Other features seen in other tourmaline crystals, in quartz crystals, and in topaz crystals may also be studied better by TEM than by topography and SID.

The topaz crystals, in which we have discovered several textural features not detectable by other techniques, should be fully studied to determine the mechanisms of strain accommodation associated with the imperfections.

A new apparatus for stressing the quartz (and other) crystals at or above the transition temperature should be designed and applied to the crystals. In fact, a proposal to obtain support for this study is in preparation. The new design of the stressing apparatus will incorporate a controllable strain-rate, read-out of the strain magnitude, and correctable friction effects. The quartz before-and-after experiments already completed provide an excellent beginning for the proposed study, because it has already been demonstrated that features can be created for correlation with naturally-occurring features in quartz crystals.

BIBLIOGRAPHY

Six references pertain to the manuscript in Appendix I and are cited there.

Fourteen references pertain to the manuscript in Appendix II and are cited there.

Additional references cited in the body of this report follow:

Hafner, S.S., M. Raymond, and S. Ghose (1970) Nuclear quadrupole coupling tensors of Al in andalusite, J. Chem. Phys., 52, pp. 6037-6041.

Lang, A.R. (1967) Fault surfaces in alpha quartz: their analysis by x-ray diffraction contrast and their bearing on growth history and impurity distribution, Proc. Int. Conf. on Crystal Growth, Boston, 20-24 June 1966, pp. 833-838.

Thomas, L.A. and W. A. Wooster (1951) Piezocrescence - the growth of Dauphiné twinning in quartz under stress, Proc. Royal Soc. London, V.208, pp. 43-62.

Tsang, T. and S. Ghose (1973) Nuclear magnetic resonance of ^{1}H, ^{7}Li, ^{11}B, ^{23}Na, and ^{27}Al in tourmaline (elbaite), Amer. Mineral., 58, pp. 224-229.

APPENDIX I

Wagner, C.E., C.O. Pollard, Jr., R. A. Young, and Gabrielle Donnay (1971) Texture variations in color-zoned tourmaline crystals, Amer. Mineral., 56, pp. 114-132.

NOTE: This a draft of a paper being submitted for publication. Contents of this paper should not be quoted nor referred to without permission of the author.

Texture Variations in Color-Zoned Tourmaline Crystals

C. E. Wagner, C. O. Pollard, Jr.

R. A. Young, and Gabrielle Donnay

Georgia Institute of Technology

Atlanta, Georgia 30332

Geophysical Laboratory

Carnegie Institution of Washington

Washington, D. C.

Abstract

Two x-ray diffraction imaging techniques have been applied for the first time to the study of previously unnoted mosaic detail in color-zoned Brazilian tourmaline. The divergence source-image distortion (DSID) technique gives maximum values for misorientations among all observable grains, whereas the convergence source-image distortion (CSID) technique yields the magnitude of misorientation between adjacent grains. Strikingly abrupt textural changes are observed; they are always accompanied by color changes. The converse is not found to hold. The central or core region of all five plates studied shows a macromosaic texture corresponding to an intrinsic rocking curve that would have a width at half height of $\sim$ 1.2 minutes of arc. No grain elongation is observed.

The core region is sharply delineated from a surrounding ring or overgrowth region of lamellar texture, in which grains approximate $(2\bar{1}\bar{1}0)$ lamellae. The lattices of the lamellae in a given region are tilted with respect to each other by angles predominately less than 5 minutes of arc but ranging up to 13 minutes of arc, the tilt axis being parallel to the long dimension of the lamella in the basal plane. The lamellar grains are subparallel in a given boundary region, and are normal to the growth boundaries on the $(01\bar{1}0)$, $(\bar{1}010)$ $(1\bar{1}00)$ faces but on the other three regions they are parallel to the lamellae on an adjacent boundary. Electron microprobe traces rule out exsolution and compositional domain structures as an explanation of lamellar texture. Sudden drastic changes in conditions controlling crystal growth are possible causes of our observations.

INTRODUCTION

Textural variations have been observed in tourmaline (Wagner, Donnay, Pollard, and Young, 1968) by a special x-ray technique, source-image distortion (SID) (Young and Wagner, 1966). The variations of interest were those between different homogenous textures in adjacent regions of single crystals showing color zones. Abrupt texture changes are always accompanied by color changes, but the converse is not true.

The possibility that characteristic texture-differences, not indicated by other methods, may be related to one or more parameters (such as growth temperature and pressure) is suggested on the basis of the work reported here which also includes lattice parameter measurements, electron microprobe analyses, optical studies in polarized light, and x-ray radiography.

SID TECHNIQUE

Because the source-image distortion (SID) technique (Young and Wagner, 1966) is not widely known, a brief summary follows, together with a description of a new modification of the technique.

Two different geometric arrangements were used. In both arrangements, the x-ray source has dimensions such that it extends only very slightly outside the plane of incidence (p.o.i.), the plane containing the incident and the scattered x-ray beam to be detected. (The normal to any diffracting set of Bragg planes also, of necessity, lies in the p.o.i.) In both arrangements sufficient cross-fire is present in the p.o.i. so that the incident beam simultaneously meets the condition for Bragg diffraction for crystal regions of slightly different orientations and interplanar spacings, d.

In the divergence SID technique (DSID) the source dimension in the p.o.i. and perpendicular to the source-to-specimen line is limited either by small source size or by a slit placed as close to the source as is conveniently possible. A variation of this arrangement uses a line source in the p.o.i. and Soller slits near the source to give the effect of several "point" sources. Thus the required cross-fire is provided in the form of divergence (Fig. 1a). In the convergence SID technique (CSID) arrangement, the source dimension measured in the p.o.i. is deliberately made large, e.g., the long dimension of a line-focus source of x-rays is placed in the p.o.i. and the limiting slit is placed as close to the specimen as possible. The required cross-fire is thereby provided as convergence (Fig. 1b).

The SID principle may be understood from consideration of either arrangement; the divergence arrangement is chosen for the more detailed discussion here. When a large planar crystal is placed in diffracting position at some distance from a point source of x-rays, not all of the crystal can diffract the characteristic wavelength simultaneously. The loci of actively diffracting portions extend in a band across the crystal. The width of this band depends on the intrinsic diffraction profile of the crystal and on the dimension of the x-ray source in the p.o.i. A film placed perpendicular to the diffracted beam at any point records the location of the diffracting regions as elongated "source images". Distortions in the crystal under examination, such as changes in lattice spacing or misalignment of grains, cause the region effectively diffracting the incident x-ray beam to be shifted across the face of the crystal (Fig. 2). It can be seen that $K\alpha_1$ and $K\alpha_2$ wavelengths are well resolved and diffract along separate bands. The band of one is badly distorted because it crossed over a region of the crystal that was warped by the mounting cement; the other one did not.

At each point, the shift of the diffracting band from its "normal" location is determined either by the component of tilt about an axis normal to the p.o.i., or by the change in spacing of the active Bragg planes or by a combination of both. The angular change produced by a strain, $\frac{\Delta d}{d}$, increases with the tangent of the Bragg angle. The contributions of tilt and strain to the distortion of the image can, therefore, be separately determined from observations made with several orders of the same reflection. They also can be separated by observations with the pair of reflections $hk\ell$ and $\bar{h}\bar{k}\bar{\ell}$ (strain will increase or decrease the apparent diffraction angle similarly for both reflections but tilt will increase the apparent diffraction angle for one and decrease it for the other.)

For crystals with narrow diffraction profiles, a single slit provides information for only a small fraction of the crystal surface. Several separate x-ray sources equally spaced along a line in the p.o.i. will have separate loci of reflection on the crystal and so may be used to sample distortions over a larger area at once. Soller slits placed in front of a line source lying in the plane of incidence produce such an effect (Fig. 3). If no significant distortion is present in the specimen, the source image consists of parallel lines (Fig. 4).

In the CSID technique (not previously reported) the defining slit is placed adjacent to the sample with the slit extending normal to the p.o.i. so that the crystal is illuminated with convergent radiation. Each specimen point in the band defined by the slit can then diffract (when the crystal is "aligned"). The film records (Fig. 5) the direction in which the diffracted ray from each point travels (with respect to the rays diffracted from the other portions of the band) and over what angular range (width of diffraction

profile). Typical dimensions are: slit width, 0.05mm; x-ray source-to-specimen distance, 12 cm (providing a maximum convergence angle of about 5 degrees); and specimen-to-film distance, 1 meter or more (to provide good resolution of angular variations). Principally, the two methods differ in that, for DSID, the active source points are fixed and the selection of active specimen points depends on the distortions present, whereas for CSID, the slit determines the active specimen points and the distortions determine the active source points.

Definition of Texture

Texture shall be taken here to mean the pattern of grain size and orientation within what would ordinarily be called a single crystal. One extreme case is that of a nearly perfect, undistorted crystal, such as the quartz plate used for Fig. 4. For the more usual case of "single" crystals with relatively few randomly-oriented microcracks and low-angle grain boundaries (Fig. 6) we will use the term "macromosaic texture." In Fig. 7 the grains are apparently elongated in at least one direction and misorientation occurs about an axis parallel to this direction. The texture of this sample will be referred to as "lamellar."

EXPERIMENTAL

General Characterization of the Tourmaline Specimens.

Some "single" crystals of minerals show evidence of heterogeneity even to the naked eye. A well known example is that of multicolored tourmaline. Electron microprobe analyses for Fe, Mn, Mg, and Al re-confirmed the correlation between color and content of Fe and Mn first reported by Bradley and Bradley (1953) on the basis of spectroscopic analyses. However, whether the correlation is with the absolute amounts present or is with the Fe-to-Mn

ratio is still not known. Qualitatively, the colors range from black to green to blue to clear to pink as the Fe-to-Mn ratio decreases.

Contact x-ray radiographs (Fig. 8) of our three largest samples showed that differences in x-ray density coincide with the differences in color.

Changes in lattice parameters were determined from doubly-exposed x-ray photographs prepared as follows: After a precession photograph was made of one small region of the sample, the film cassette was raised slightly, the crystal was translated parallel to itself to expose a different region of interest and a second photograph was made on the same film. Uncertainities due to film shrinkage were thereby eliminated. The method could also reveal misalignment between the exposed regions (Donnay, 1968). Two sections cut from one crystal of Brazilian tourmaline exhibiting a pink region and a blue region and sections from several other similar tourmaline crystals were so examined. Within a region of a single color, lattice parameter differences of 0.4% were observed for a; between differently colored regions differences as large as 0.8% in a and 0.3% in c were observed, even though the samples appeared to be single crystals under the usual x-ray and optical examinations.

SID Studies of Tourmaline Crystals

Initial studies were undertaken to ascertain what, if any, strains accompanied the change in color (i.e., in chemical composition) at a color-zone boundary. DSID studies were made on (i) approximately 1 mm thick (00.1) sections of three tourmaline crystals of Brazilian origin (crystals B1-B3) and (ii) on a (00.1) section (B4) and a ($1\bar{2}.0$) section (V1) so cut from the same Brazilian tourmaline crystal that they were nearly contiguous. B4 and V1 were about 0.2 mm thick.

All samples were polished and etched to remove surface strains. Each sample exhibited at least one strong color difference between color zones.

Section B1 came from a crystal with a large blue core and a narrow clear rim. B2 came from a crystal color-zoned (from core to rim) dark green to pink to light green. B3 was cut from a crystal that had a core of one shade of pink over-grown with a zone of darker pink grading to light pink which, in turn, gave way to a medium-green rim. B4 and V1 were taken from a crystal that was zoned from light green in the center to pink to light green at the rim.

Sample B3

A 00.3 (symmetric Bragg case) DSID pattern of specimen B3 is shown in Fig. 9. Two regions of distinctly different texture are detectable. In the central (pink) region of the specimen the $K\alpha_1$ and $K\alpha_2$ bands were slightly distorted in various directions as a consequence of the macromosaic texture. The diffracted images (the dark bands) were about 0.5 mm wide (unmagnified). Knowing the instrument dimensions, one could then deduce that the intrinsic rocking curve of this portion of the sample has a width at half height of about 3.6×10^{-4} radians or 1.2 minutes of arc.

From the character of the top of the image one sees, in the portion corresponding to the green region of the crystal, that the individual diffracting areas are much smaller than those in the pink region and that they are elongated and usually extend the entire width of the green region. Each individual distinct area of the image arises from a different grain and we conclude that in this outer region the grains have an elongated dimension in the basal plane (00.1). These grains are shown below to be lamellae; therefore, this texture is designated "lamellar texture." From patterns made with higher order reflection (00.6 and 00.9) it was determined that the distortions producing the characteristic textures were primarily tilts rather than strains. In any particular exposure the observable tilts were those with

a component about an axis normal to the p.o.i. (i.e., and axis parallel to the SID lines), as mentioned above; thus it could be determined from the DSID pattern of Fig. 9 that the lamellar grains were misoriented, with a rotational component of 13 minutes of arc or less about a line parallel to the apparent elongation direction of the grains.

The crystal, B3, was then rotated 90° about the c direction and a 00.6 DSID pattern was obtained (Fig. 10). Since the same lamellar grains observed in Fig. 9 are not delineated in Fig. 10, it can be concluded that there were no significant mirorientations about that axis which is (i) normal to the long direction of the grain image in Fig. 9 and (ii) lies in the plane of the slice.

The other rim portions of this crystal yield similar results for their grains: (i) The grain cross-sections were elongated, (ii) in most cases the grains extended the entire width of the green region, and (iii) the grains were misoriented about an axis approximately parallel to the long dimension of their observed cross-sections and (iv) the angle of misorientation was usually not more than 5 minutes of arc and was very rarely more than 10 minutes of arc.

Samples B1 and B2

Similar results were obtained for the textures of the other basal sections, but a particular color could not be correlated with a particular texture. For instance, the lamellar-textured rim of B3 is light green and the central region is pink, but in specimen B2 lamellar textures were shown by both pink and light green rims about a dark green core. Cores never contained lamellar grains. Representative 00.3 DSID patterns of the three thicker samples (B1, B2, B3) are shown in Fig. 11

The core regions often have roughly hexagonal cross-section in the basal plane, but the long dimensions of the grain cross-sections are perpendicular to the three overgrowth boundaries, $(01\bar{1}0)$, $(\bar{1}010)$ and $(1\bar{1}00)$, but are not perpendicular to the $(0\bar{1}10)$, $(10\bar{1}0)$ and $(\bar{1}100)$ boundaries. Instead, the lamellae on the latter three boundaries are parallel to the lamellae perpendicular to one of the adjacent overgrowth boundaries. On a given boundary there was but one orientation of the lamellar grains.

Sample B4

Sample B4 was thin enough to permit multiple source, transmission DSID patterns to be made without overlap of grain images (Fig. 12). The difference in textures between core and outer regions is more clearly shown here than in the preceding figures, as are the individual grains. However, the textures of this sample are similar to those of the other basal sections.

Sample V1

Because samples V1 and B4 were nearly contiguous, the extent of the rim grains in the c direction could be investigated. The evidence for the elongation parallel to c and for the lack of rotation about the c direction was obtained exclusively from this sample pair. Fig. 13 is a multiple source, transmission DSID pattern of V1 obtained with the 33.0 reflection. The color and texture boundary observed in B4 occurs along a line joining the arrows, with the highly-textured rim region lying on the left. This sample has a large number of (optically) visible cracks which obscure the SID x-ray data. Near the left edge there are few, however, so the distortions of the SID lines there are due to other causes. To the left of the color boundary, striations of the SID lines similar to the ones observed in the top of Fig. 12 are present. The misorientation between striated regions is less than 10 seconds of arc. Since the striations are similar in size and appearance to

those in the basal section it is assumed that they are the $(1\bar{2}.0)$ (vertical) cross-sections of the grains in the basal plane. The absence of significant misorientations about the c direction indicates the only misorientation axis lies in the basal plane and further supports correlations with the elongated grain cross-sections in Fig. 12.

Model for textural variations

A model for the texture of the samples has thus been determined: there is, first, a core region with a macromosaic texture. Second, there is an overgrowth region having approximately the same crystallographic orientation as the core; however, the overgrowth region is composed of lamellar grains crystallographically misoriented with respect to each other by rotations of up to 13 minutes of arc but generally less than 5 minutes of arc about an axis lying in an a* direction. The large dimensions of the lamellae lie in that a* direction containing the axis of misorientation, and in the c direction. In specimen B4 and V1 the lamellae thicknesses are relatively uniform at about 0.04 mm.

Amount of lamellar tilt

Differences in orientation between adjacent lamellae were determined quantitatively with the CSID technique to see if any pattern of misorientation could be detected. None could be found. Basal sections were used and the reflecting planes, p.o.i., and slit orientations were chosen so that the lamellae made slight angles with the illuminated band. This configuration maximized the probability that a significant segment of the illuminated band would fall simultaneously on two neighboring lamellae. Near maximum separation of the doubled images was achieved when the axis of misorientation was placed normal to the p.o.i. Only when two images for each wavelength were obtained from a segment of the illuminated band was it assumed that two

different lamellae were diffracting; a simple discontinuity in an image could as readily be assigned to a crack within a lamella as to a simultaneous illumination of adjacent lamellae.

Fig. 14 is a 60.0 CSID pattern of specimen B4. In Fig. 14 evidence for numerous cracks appears and numerous strained regions are indicated by slight widening of the line images. In the region between A and A' two grains diffract simultaneously. Separations of images such as those at A-A' constitute the proof of misorientation. Several CSID patterns were made and all misorientations (approximately 10) so observed ranged from a minimum of 20 seconds to a maximum of 5 minutes of arc. The minimum detectable misorientation is approximately 10 seconds of arc. The CSID patterns reveal misorientations between adjacent lamellae, whereas misorientations reported from DSID patterns are maximum values for misorientations among all the lamellae.

Petrographic Observation of Lamellae

With the SID results in mind, one could discern the rim lamellae under the petrographic microscope, but only on specimen B2 (Fig. 15). Traces of the lamellae were discernible under crossed nicols when the traces were within several degrees of the 45° position to the polarization directions. Rotation of the stage, the polarizer, or the analyzer after the position of visibility was attained only decreased the resolution of the lamellae.

Visual correlation of lamellae observed by the SID method with those observed by optical methods was possible for limited portions of the rim. A complicating factor in this effort was the oblique projection angle for the images on the SID photographs. It was found that two slide projectors, from which the separate SID and optical images on suitable transparences could be projected side-by-side from different focal lengths and different

angle, were of great help in our efforts to correlate x-ray and optical images.

DISCUSSION

The observation of greatest interest in this study is that two distinctly different textures are associated with specific regions of a "single" crystal. In each of the samples observed, the core region had a macromosaic texture containing some small cracks whereas the overgrowth region was composed of lamellar grains. No case was observed in which the core was composed of the lamellar grains, nor was a macromosaic region found as an overgrowth to a lamellar region.

Possible models consistent with the lamellar texture of the overgrowths include the following: (1) twin lamellae, (2) exsolution lamellae, (3) domain structures (including compositional domains; e.g., sector zones), and (4) deformation lamellae. None are satisfactory. No twin operation with reasonably low indices could develop the sub-parallel aggregates of the lamellar regions. The possibility that the lamellar grains might be exsolution lamellae or compositional domains can be ruled out on the basis of electron microprobe traces (for Fe, Mn, Mg and Al) made within lamellar regions of a single color. If exsolution or compositional domains had caused the lamellae, such traces would show a spatial dependence of chemical composition with the same repeat distance as the lamellae repeat distance. No such dependence was found with a 3 micron diameter microprobe beam. Domain structures other than compositional domains have not been ruled out; in fact, the lamellar texture could fairly be described as orientational-domain structure (which description gives no clue to the genesis). Deformation lamellae, such as have been reported in quartz (Bailey, Bell and Peng, 1958) and olivine (Challis, 1968), are mentioned as a possibility here only because of the similarity of their microscopic appearance to that of the rim lamellae. No suggestion that deformation might have given rise to the lamellae is intended, especially not in view of the orientations of the rim lamellae.

Color changes always accompanied texture changes but they also occurred elsewhere. There appeared to be no strict correlation between a particular

color and a particular texture. For example, in sample B2 the pink (overgrowth) region had the lamellar texture whereas in B3 the pink (core) portion had the macromosaic texture. The microprobe work has shown the Fe-to-Mn ratio to be associated with color and the Mn and Al concentrations to have only small variations that are independent of color. The radiographs have shown that the absolute concentration of heavy elements is not associated with a particular texture. Thus it appears that chemical compositions, both relative and absolute, play a merely coincidentally associative, and not a causative, role in texture formation.

If the above possibilities are excluded, as they apparently should be, then texture must be indicative of some parameter to which the more established techniques, other than SID and related techniques, are not sensitive. One may then seriously entertain the conjecture that the texture changes are indicative of some growth parameter such as temperature, pressure, or others which affect growth rate.

ACKNOWLEDGEMENTS

We thank Mr. Earl Williams of the Johns Hopkins University for supplying the tourmaline specimens and for cutting and polishing the plates.

REFERENCES

Bradley, J.E.S., and Olive Bradley (1953) Observations on the Coloring of Pink and Green Zoned Tourmaline. Min. Mag., 30 26-38

Bailey, S. W., R. A. Bell, and C. J. Peng (1958) Plastic Deformation of Quartz in Nature. Bull. Geol. Soc. Amer., 69, 1443-1446

Challis, G. A. (1968) X-ray Study of Deformation Lamellae in Olivines of Ultramafic Rocks. Mineral Mag., 36, 195-203

Donnay, Gabrielle (1968) Crystalline Heterogeneity: Evidence from Electron Probe Study of Brazilian Tourmaline. Annual Report of the Director, Geophysical Laboratory, Carnegie Institution Yearbook, No. 67, 219-220

Wagner, C. E., G. Donnay, C. O. Pollard, Jr., and R. A. Young (1968) Textural Variation in Colored Tourmaline Crystals. Amer. Cryst. Assoc. Meeting, abs. No. LL8 , August, 1968.

Young, R. A. and C. E. Wagner (1966) X-ray Source-image Distortion Technique for the Study of Crystal Distortion and Vibration. J. Appl. Phys. 37, 4070-4076

Fig. 1 (a) Divergence and (b) convergence SID arrangements.

Fig. 2 Single source divergence SID pattern showing diffracting regions for $K\alpha_1$ and $K\alpha_2$ wavelengths. A bending of the crystal produced the deformation of the diffracting regions.

Fig. 3 Experimental arrangement for the multiple source, divergence SID experiment. Source-to-specimen distance is typically 1 meter. Each beam, indicated in the Fig. by a single line, is actually divergent to the degree permitted by the length and spacing of the Soller slits.

Fig. 4 Multiple source, divergence SID pattern of a perfect, undistorted quartz crystal.

Fig. 5 Single slit, transmission, convergence SID pattern of a crystal exhibiting a discontinuity in the $K\alpha_1$ and $K\alpha_2$ images due to several small cracks. The $K\alpha_1$-$K\alpha_2$ separation is 2.8 minutes of arc. The slit in front of the specimen was 0.05 mm, the source-to-film distance 1 meter.

Fig. 6 Single slit, Bragg case, divergence SID pattern of a single grain exhibiting cracks and some broadening of the diffracted images of the $K\alpha_1$ and $K\alpha_2$ wavelengths.

Fig. 7 Single slit, Bragg case, divergence SID pattern of a highly textured sample. This texture will later be identified as "lamellar".

Fig. 8 X-ray radiographs of samples B1, B2, and B3. The x-ray source was a microfocus generator operating at 25KV.

Fig. 9 Single slit 00.3 reflection (symmetric Bragg case), divergence SID pattern of specimen B3. The slit width was 0.8 mm, the source-to-specimen distance 134 cm, the crystal-to-film distance 3 cm, and the copper x-ray tube was operating at 50 KV.

Fig. 10 Single slit, 00.6, reflection divergence SID pattern of specimen B3, with the p.o.i. rotated 90° about the surface normal from its position in Fig. 9. The lack of delineation of the grains on the right-hand edge in the figure, which was at the top of Fig. 9 means there is no misorientation of these grains about an axis parallel to that core-over-growth boundary. (The second image in the lower right corner is a reflection from a different set of Bragg planes.)

Fig. 11 Representative single slit, 00.3 reflections, divergence SID patterns of samples B1, B2, and B3 in approximately the same orientations as the crystals themselves in Fig. 8. Experimental conditions are the same as for Fig. 9. Magnification is approximately the same as for Fig. 8.

Fig. 12 Multiple source, 60.0 reflection (symmetric transmission), divergence SID pattern of sample B4. The source-to-crystal distance was 100 cm, and the crystal-to-film distance 15 cm. A high intensity molybednum target operating at 50 KV and 40 ma was used.

Fig. 13 Multiple source, 33.0 reflection (symmetric transmission), divergence SID pattern of sample V1 obtained under the same conditions as the pattern in Fig. 12. The c-axis is here vertical. The color change occurs along a line joining the arrows.

Fig. 14 Convergence SID pattern of specimen B4. Molybdenum $K\alpha_1$ and $K\alpha_2$ images for the 60.0 reflection are shown. The source-to-slit distance was 12 cm, crystal-to-film distance 100 cm, and the slit width was 0.05 mm.

Fig. 15 Petrographic photomicrograph of specimen B4 between crossed Nicols. The color boundary is shown in the lower left corner. The suspected lamellar features are the bands that run from the lower left to the upper right corners. Magnification is approximately 90X.

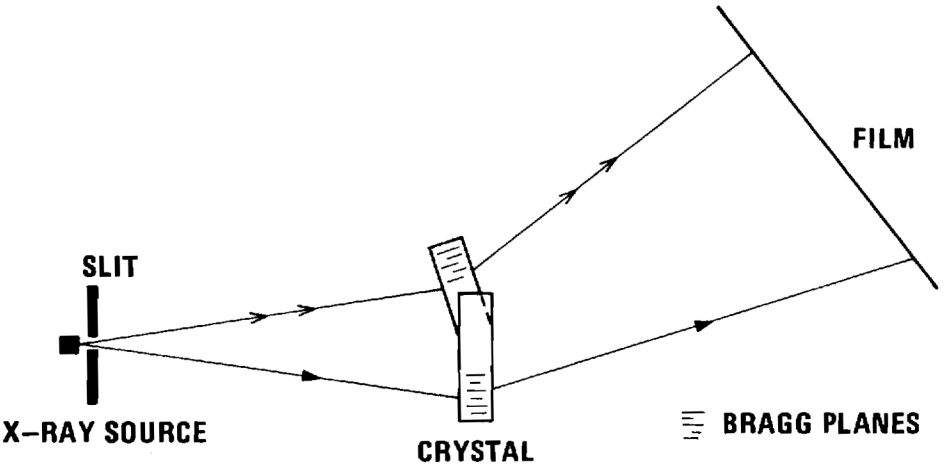
FILM
SLIT
X–RAY SOURCE
CRYSTAL
BRAGG PLANES

(a)

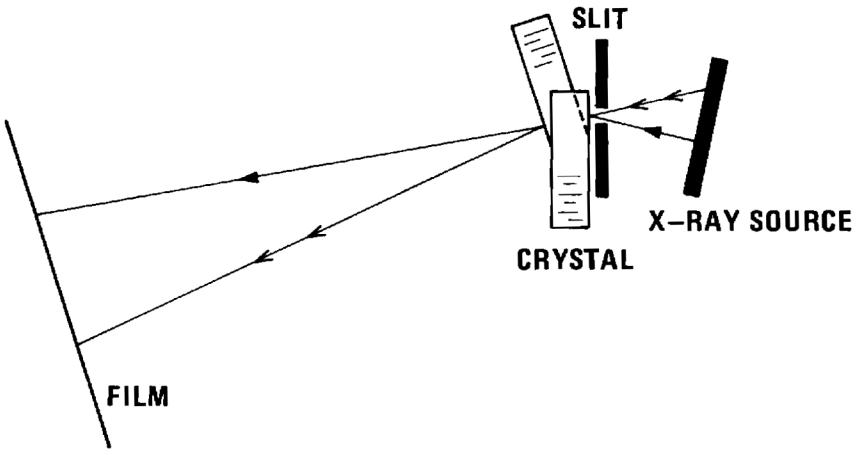
SLIT
X–RAY SOURCE
CRYSTAL
FILM

(b)

Figure 1.

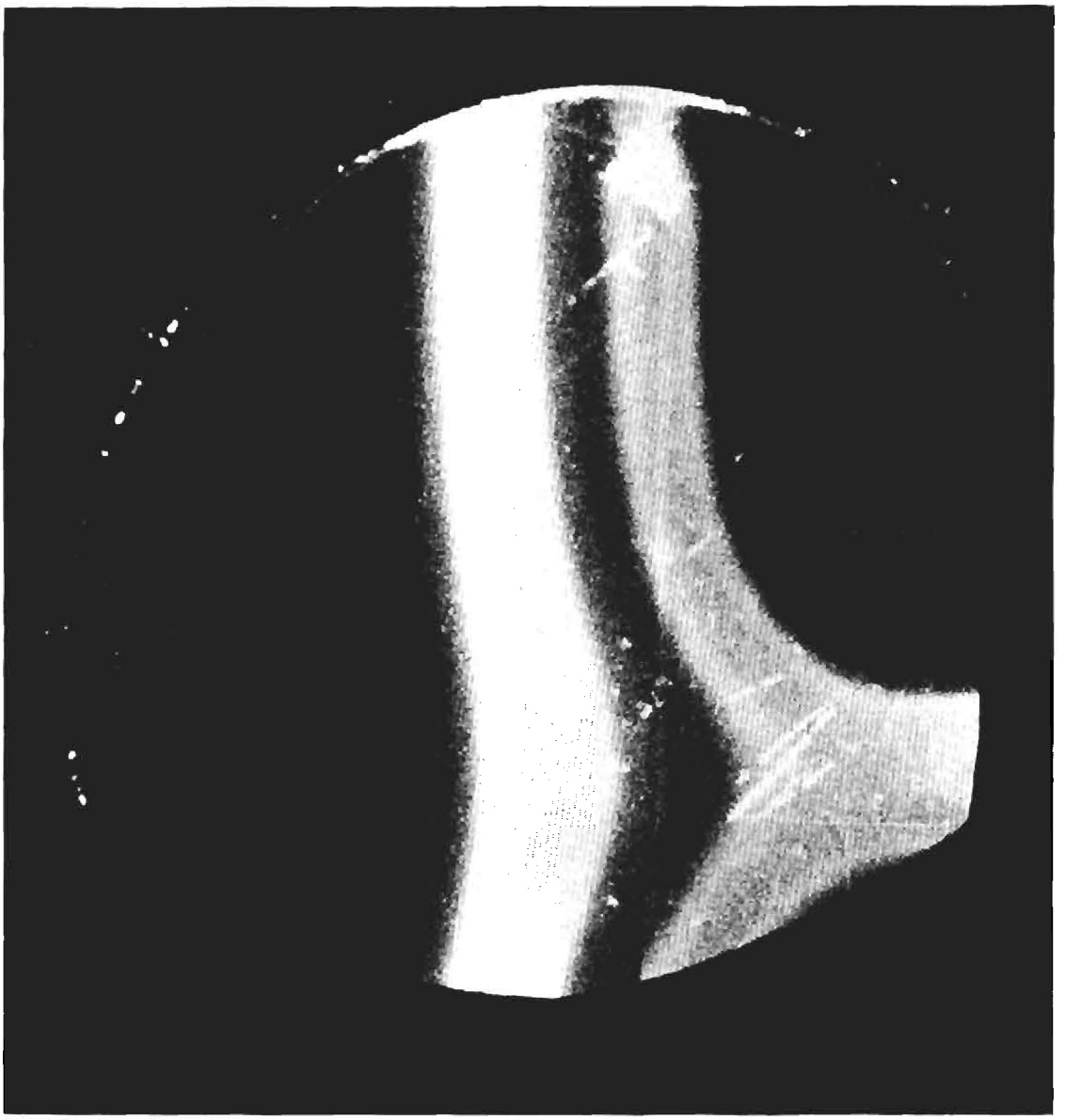

Figure 2.

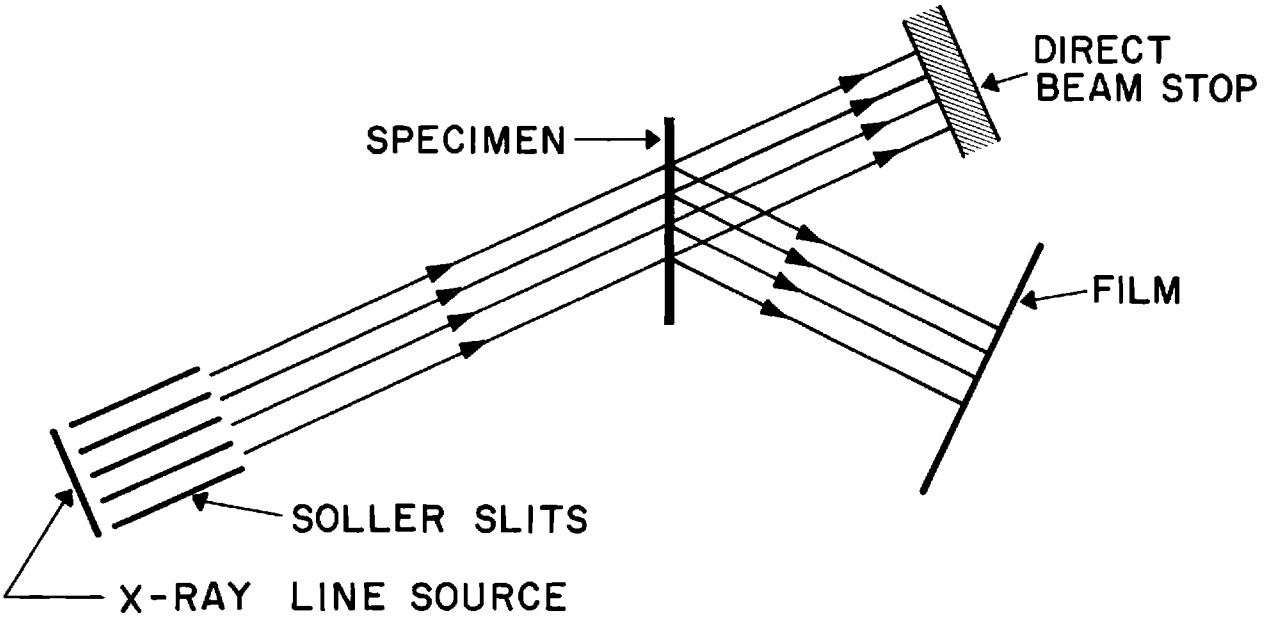
DIRECT
BEAM STOP
SPECIMEN
FILM
SOLLER SLITS
X-RAY LINE SOURCE

Figure 3.

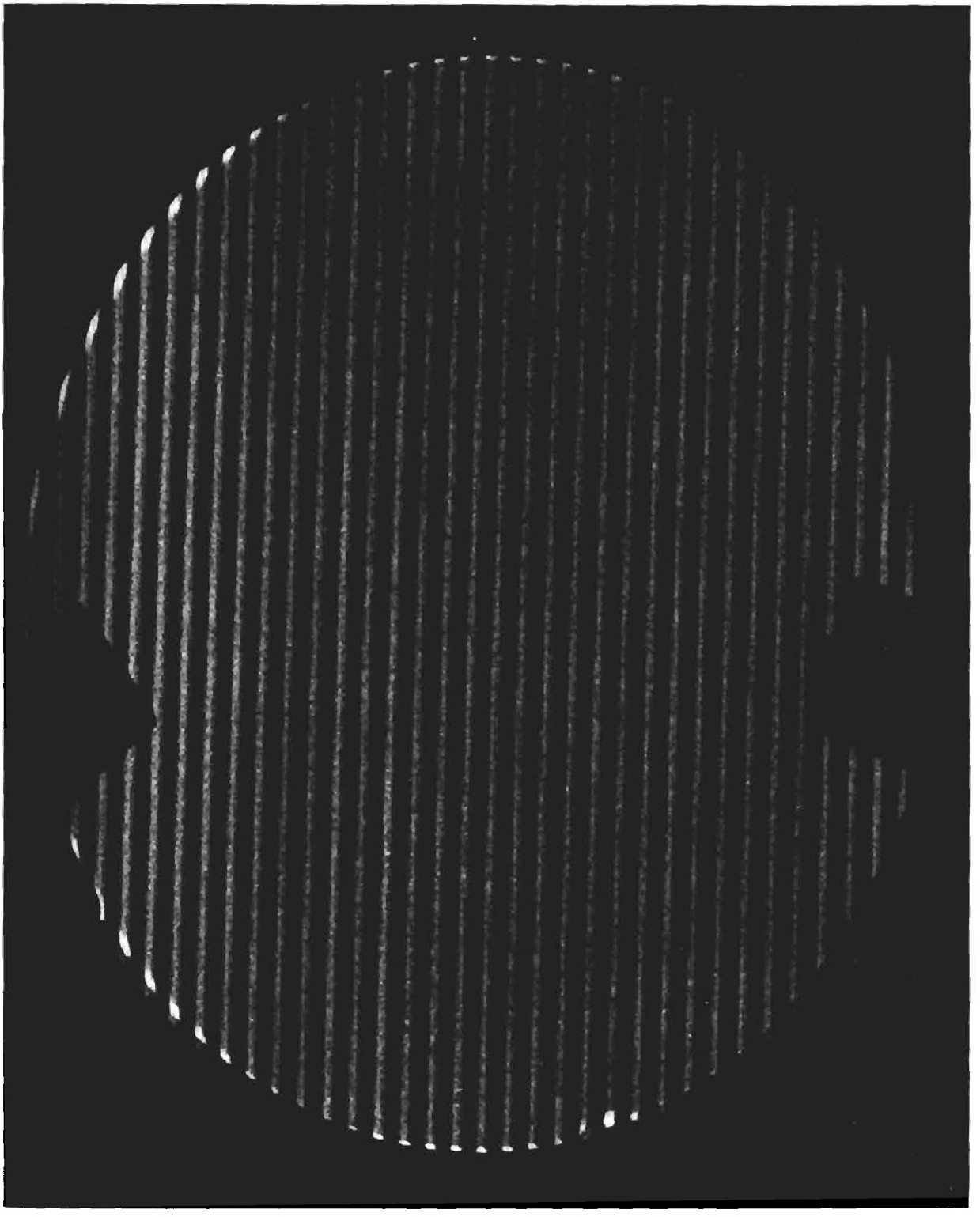

Figure 4.

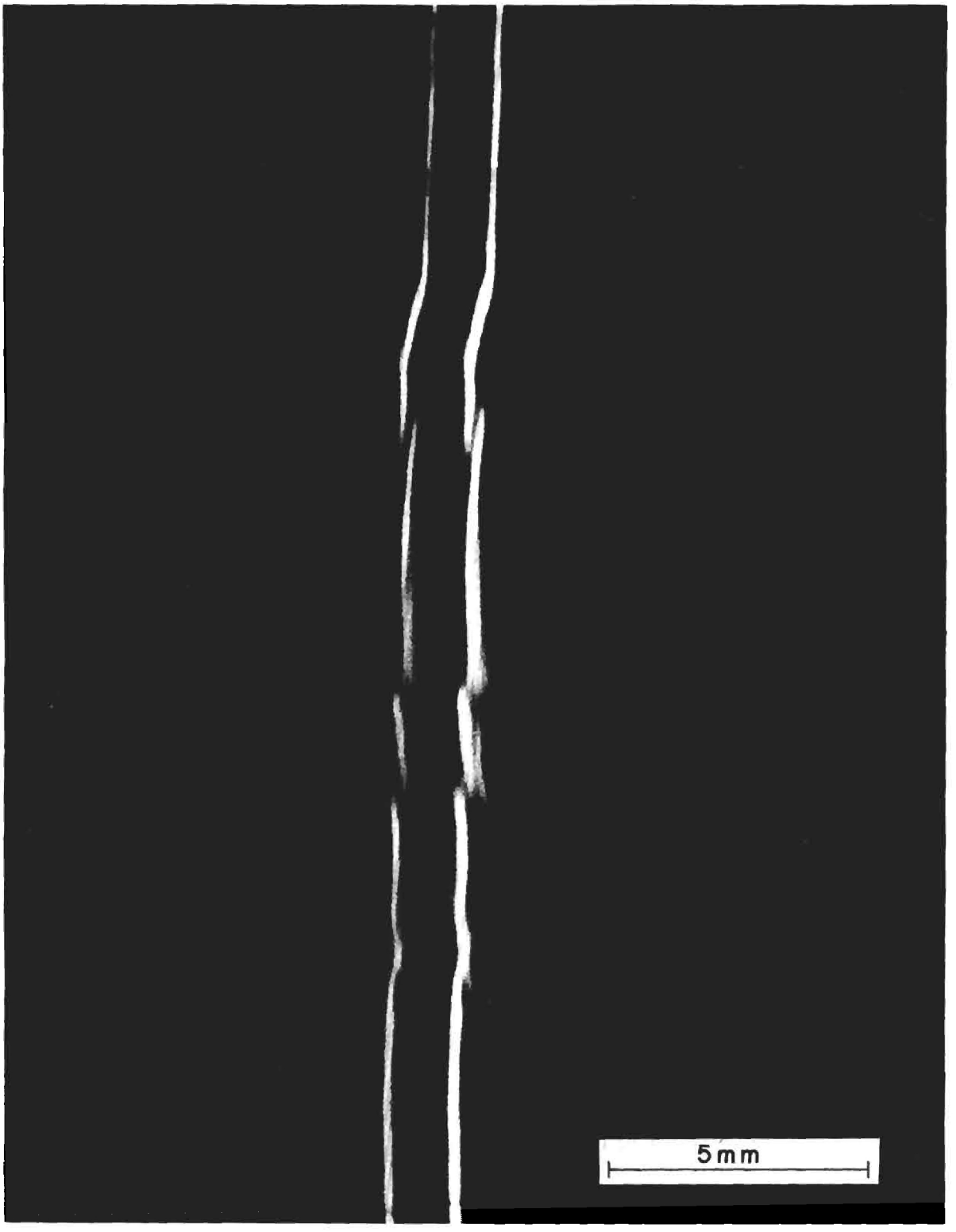

Figure 5.

Figure 6.

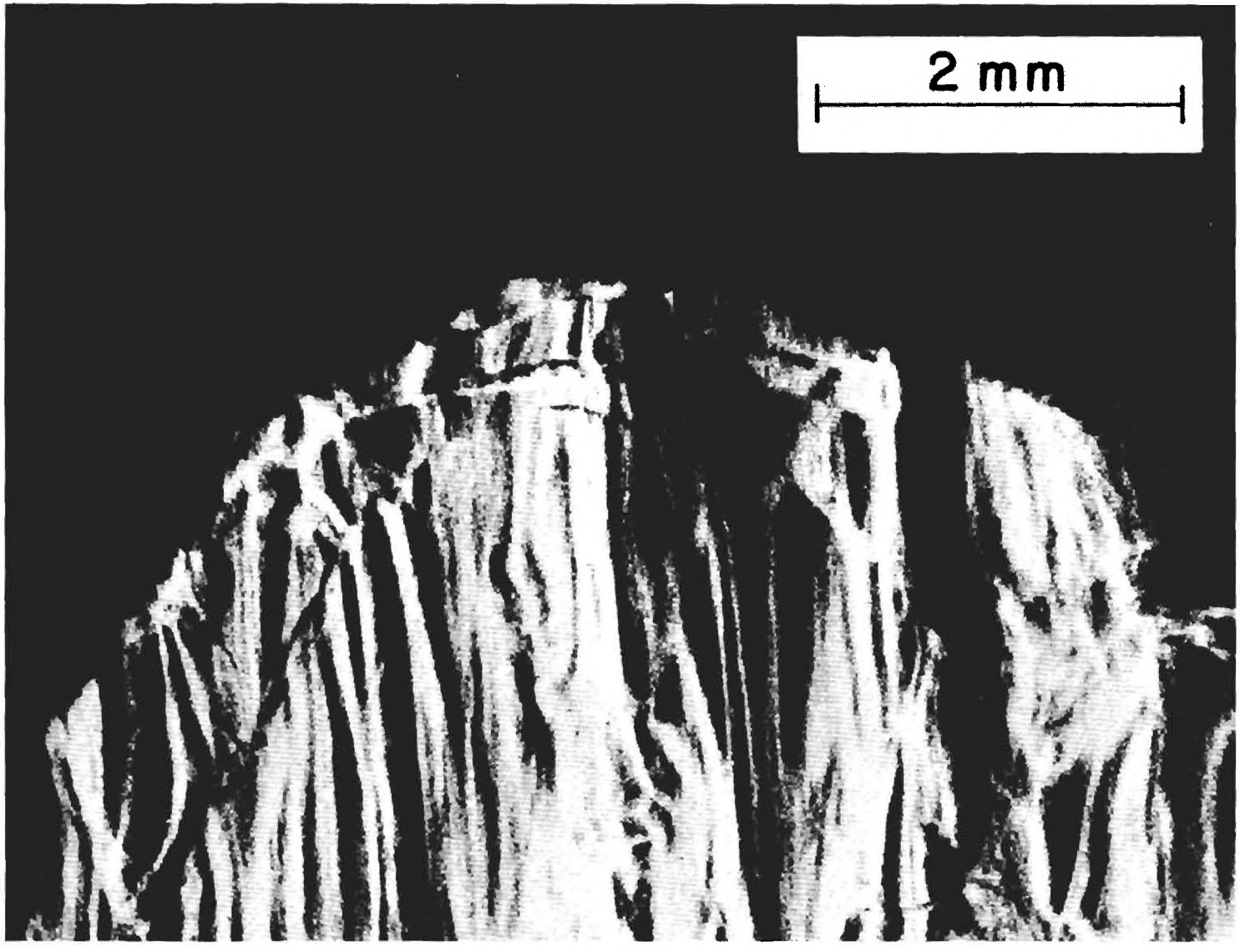

Figure 7.

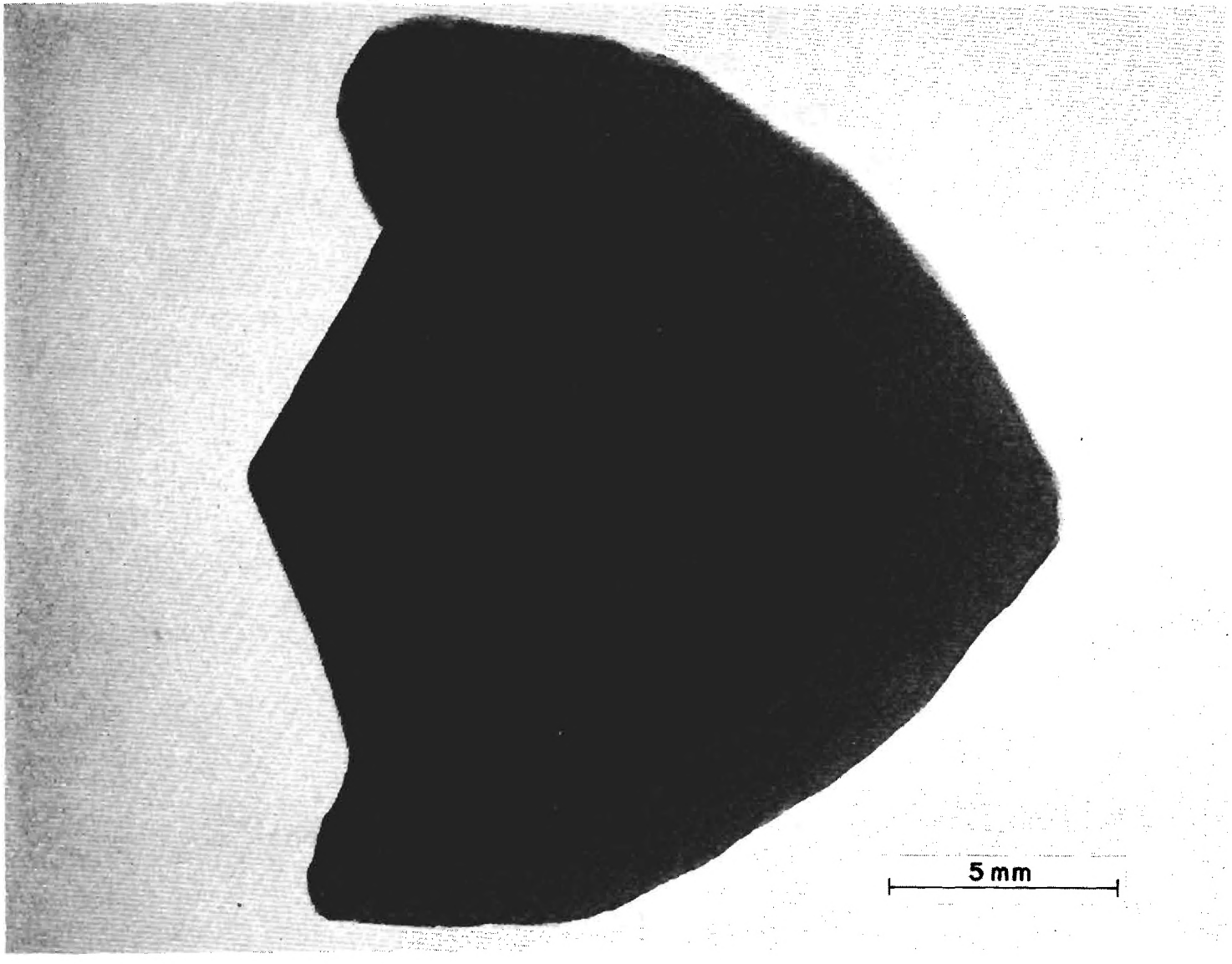

Figure 8a.

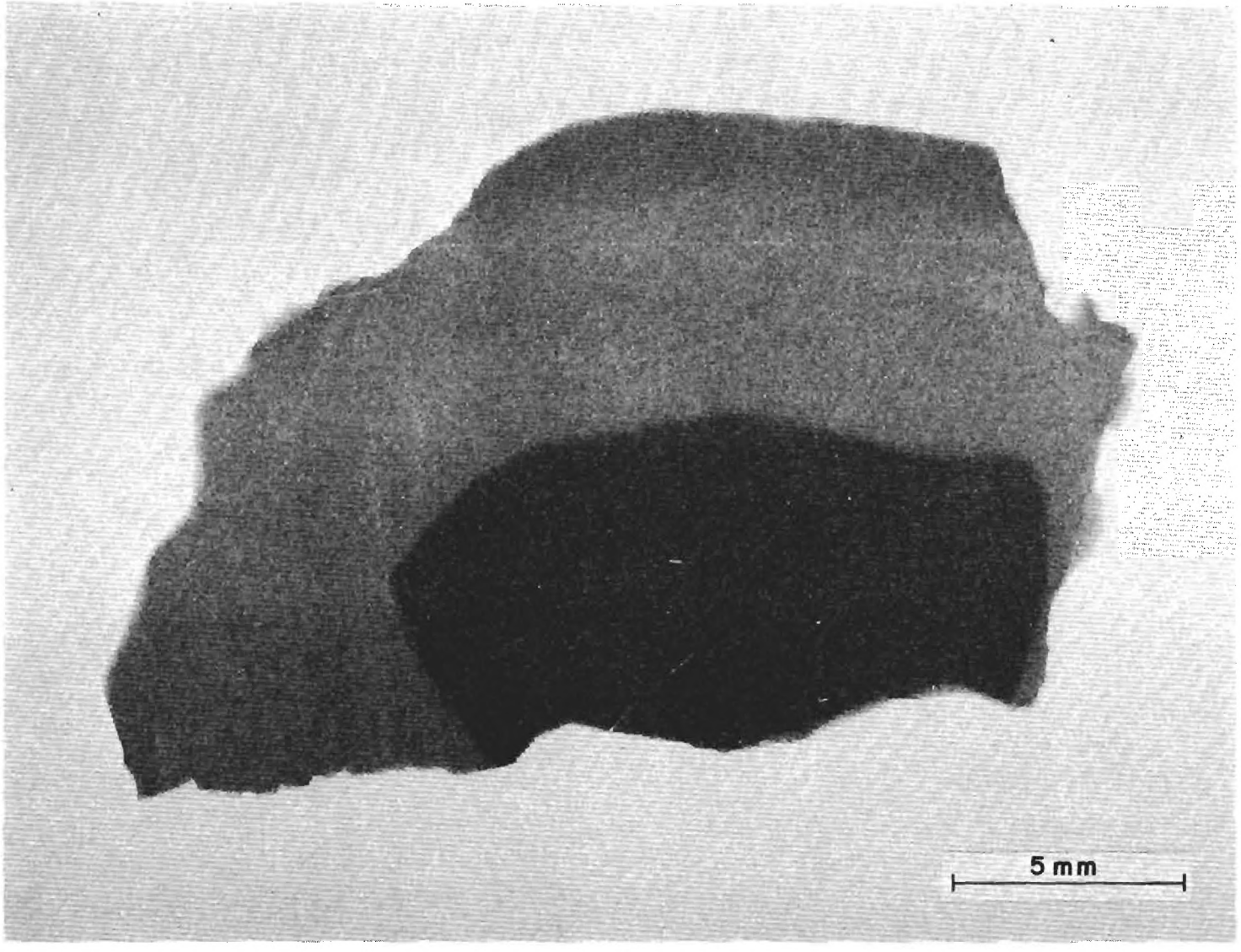

Figure 8b.

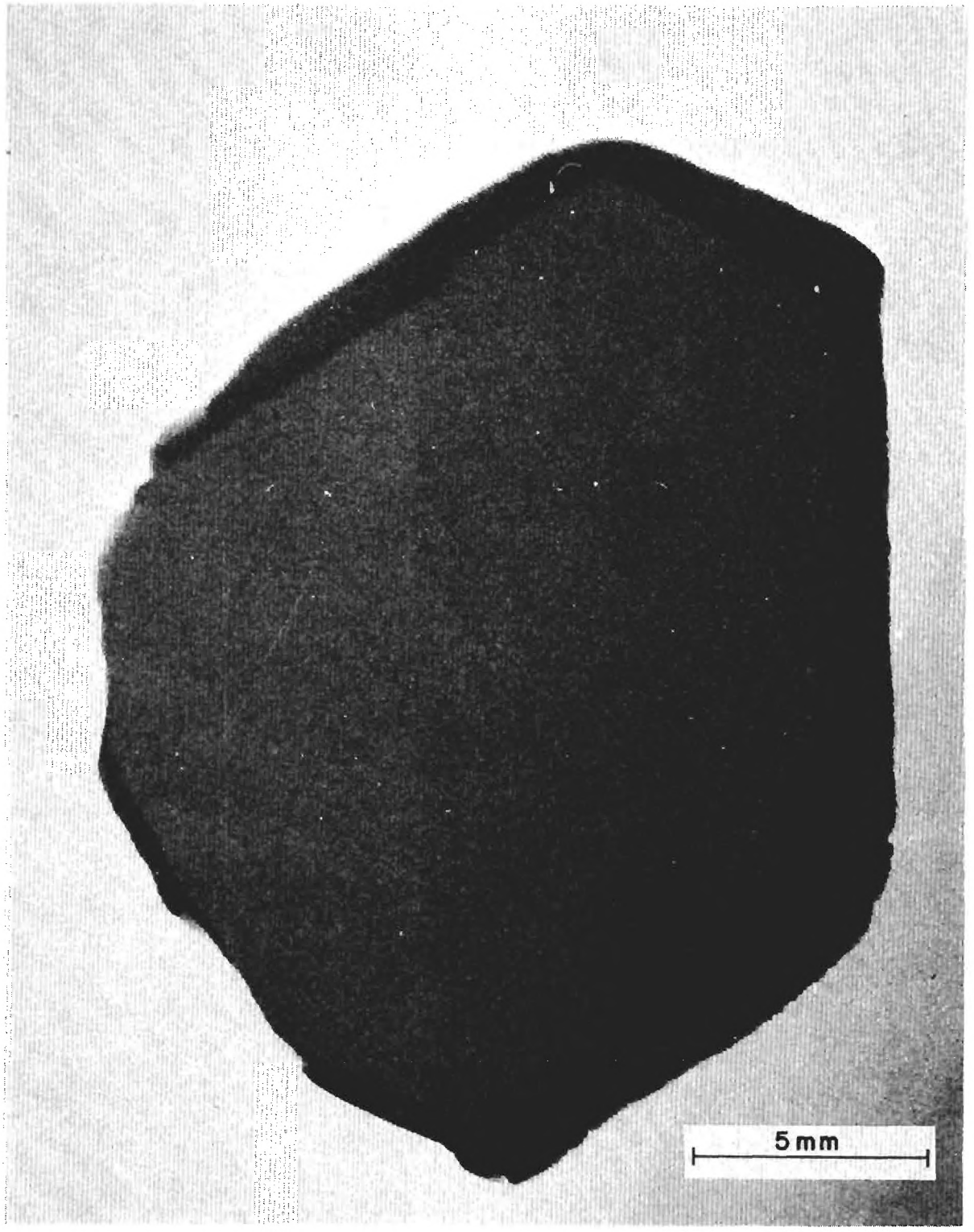

Figure 8c.

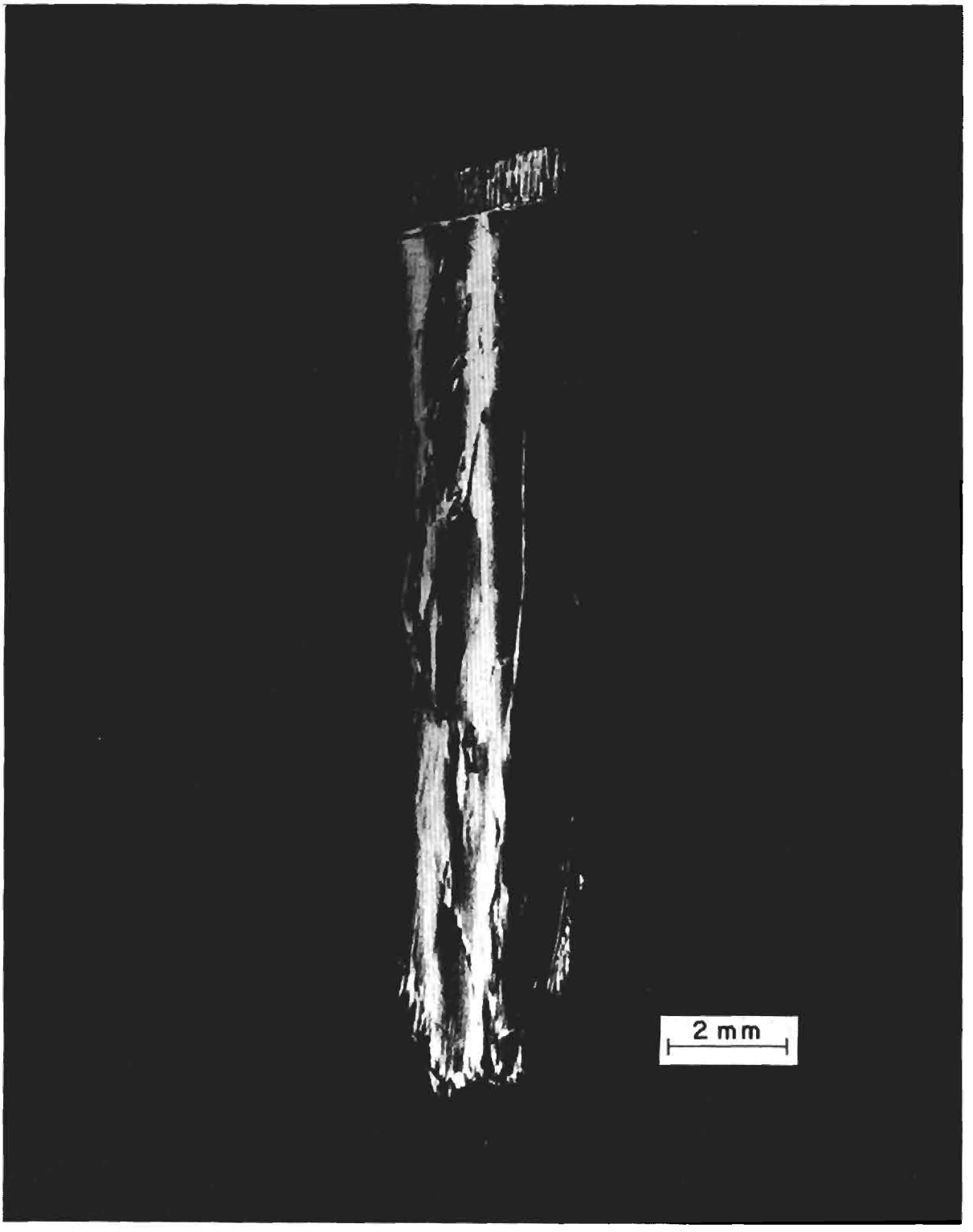

Figure 9.

Figure 10.

Figure 11a.

Figure 11b.

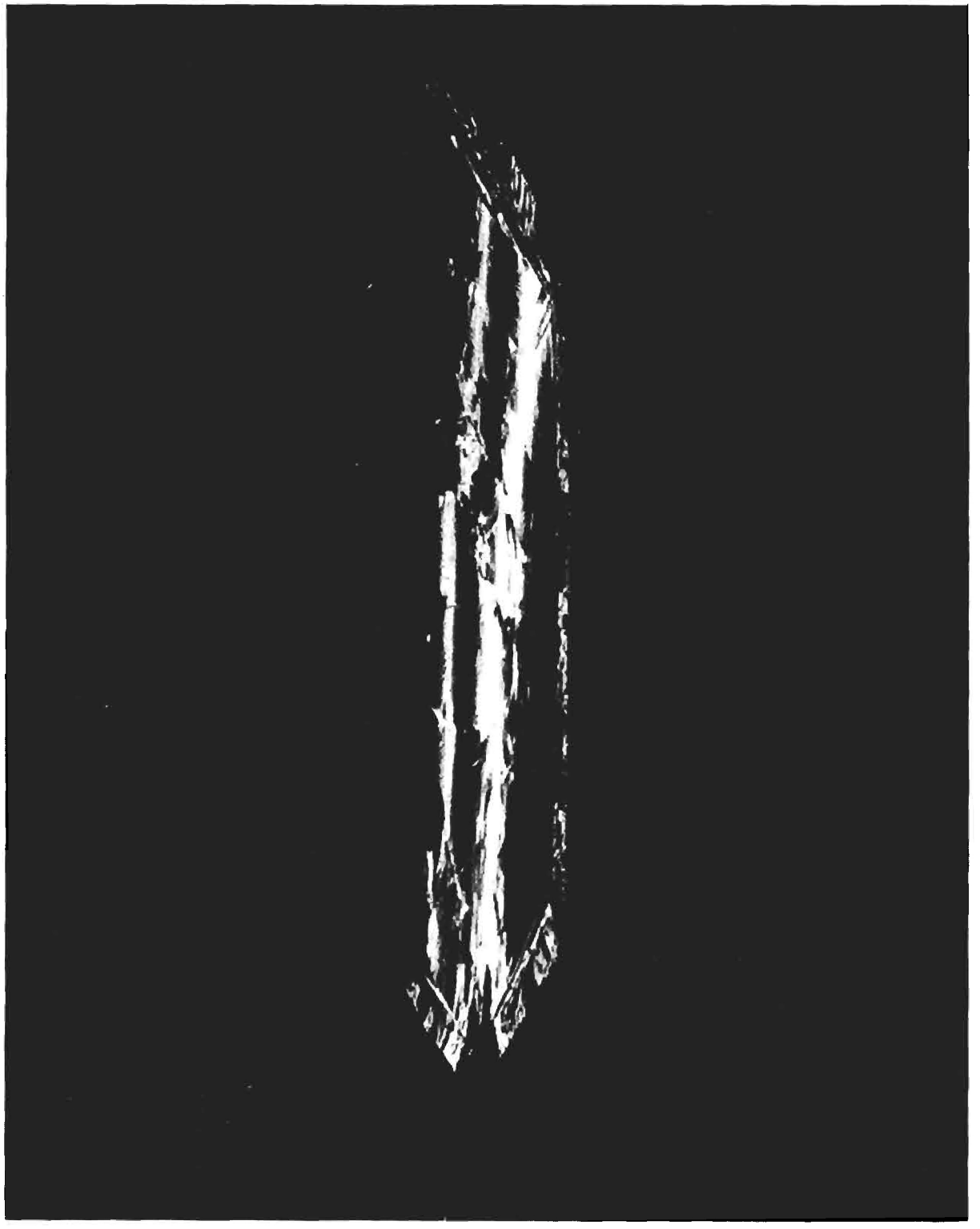

Figure 11c.

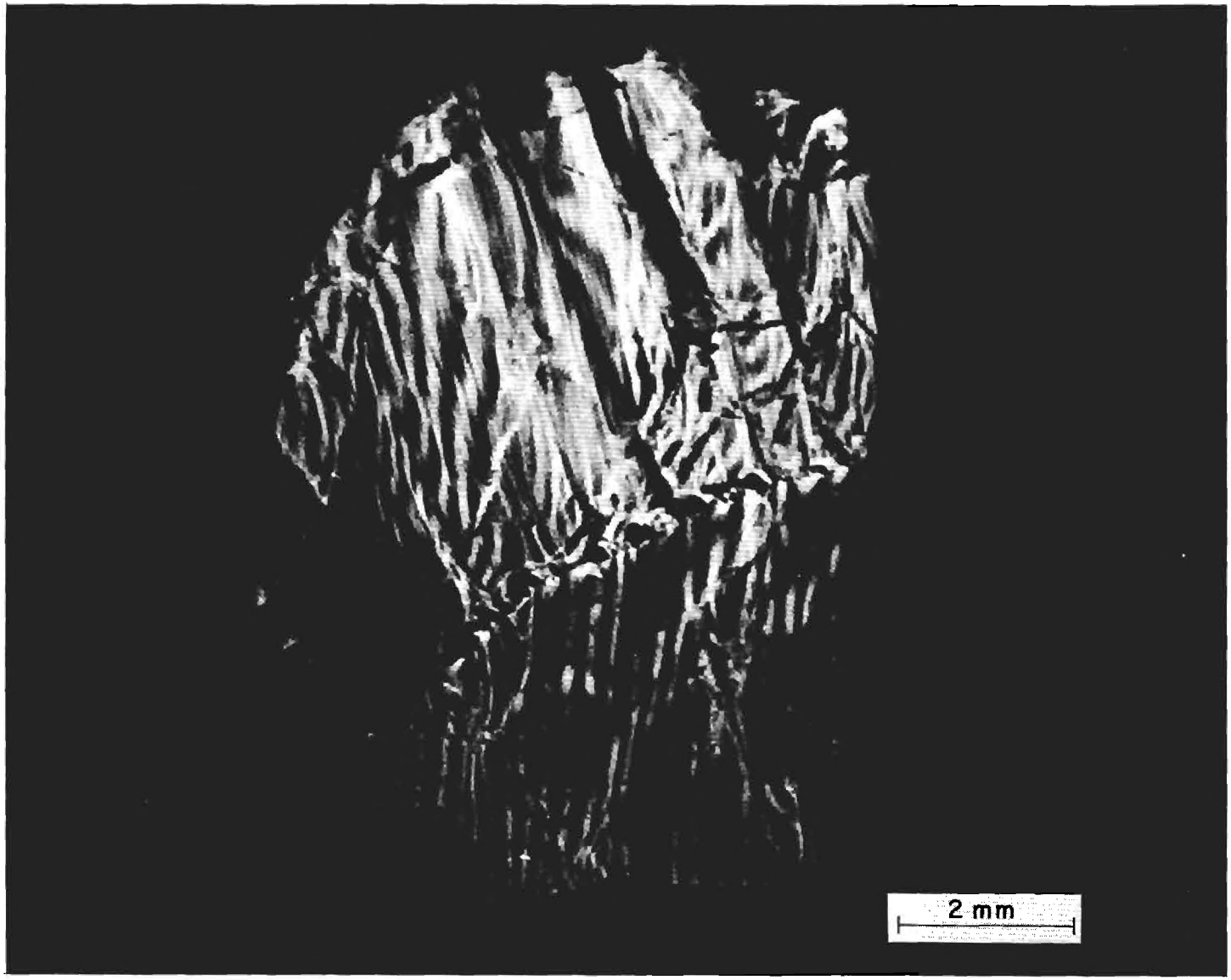

Figure 12.

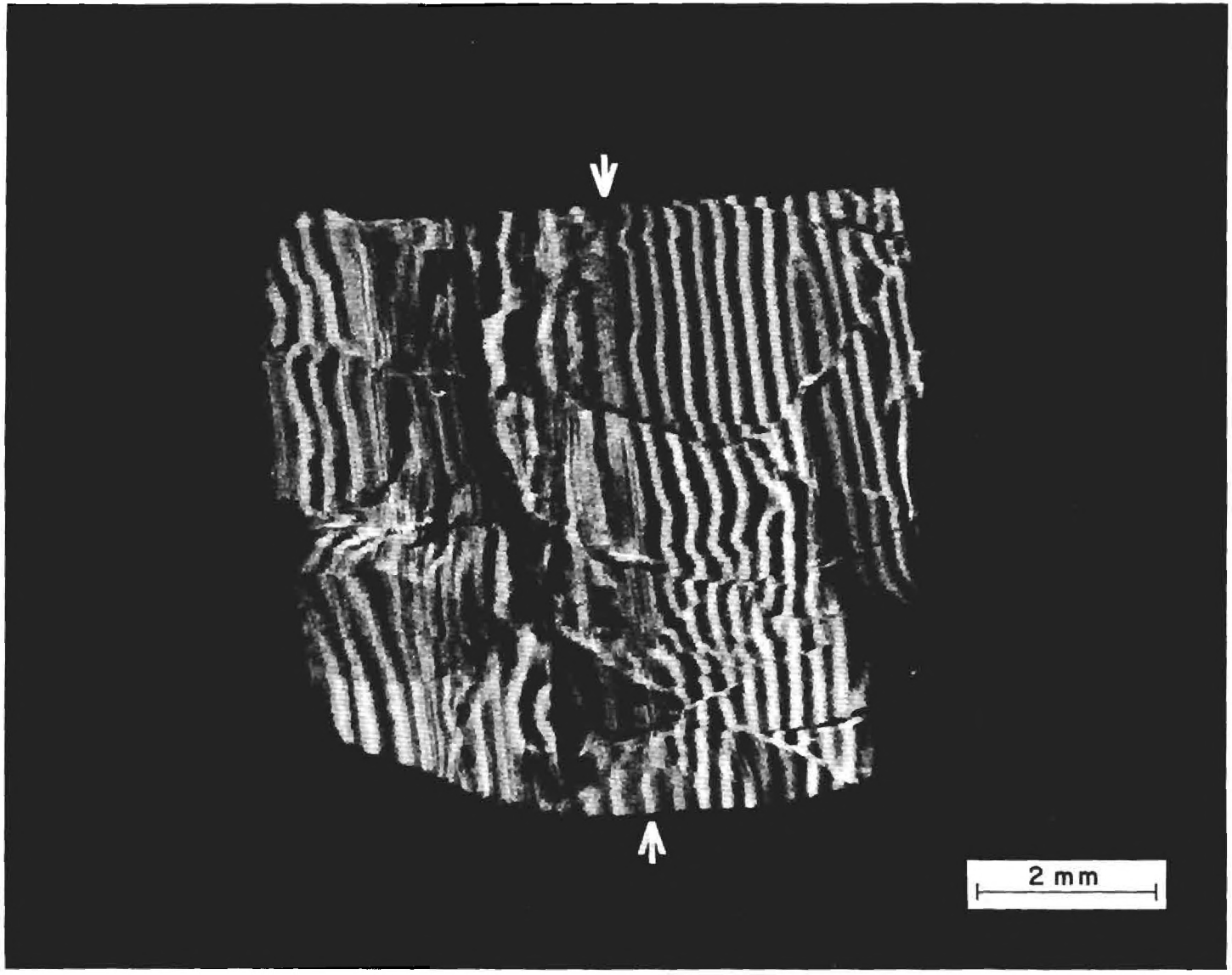

Figure 13.

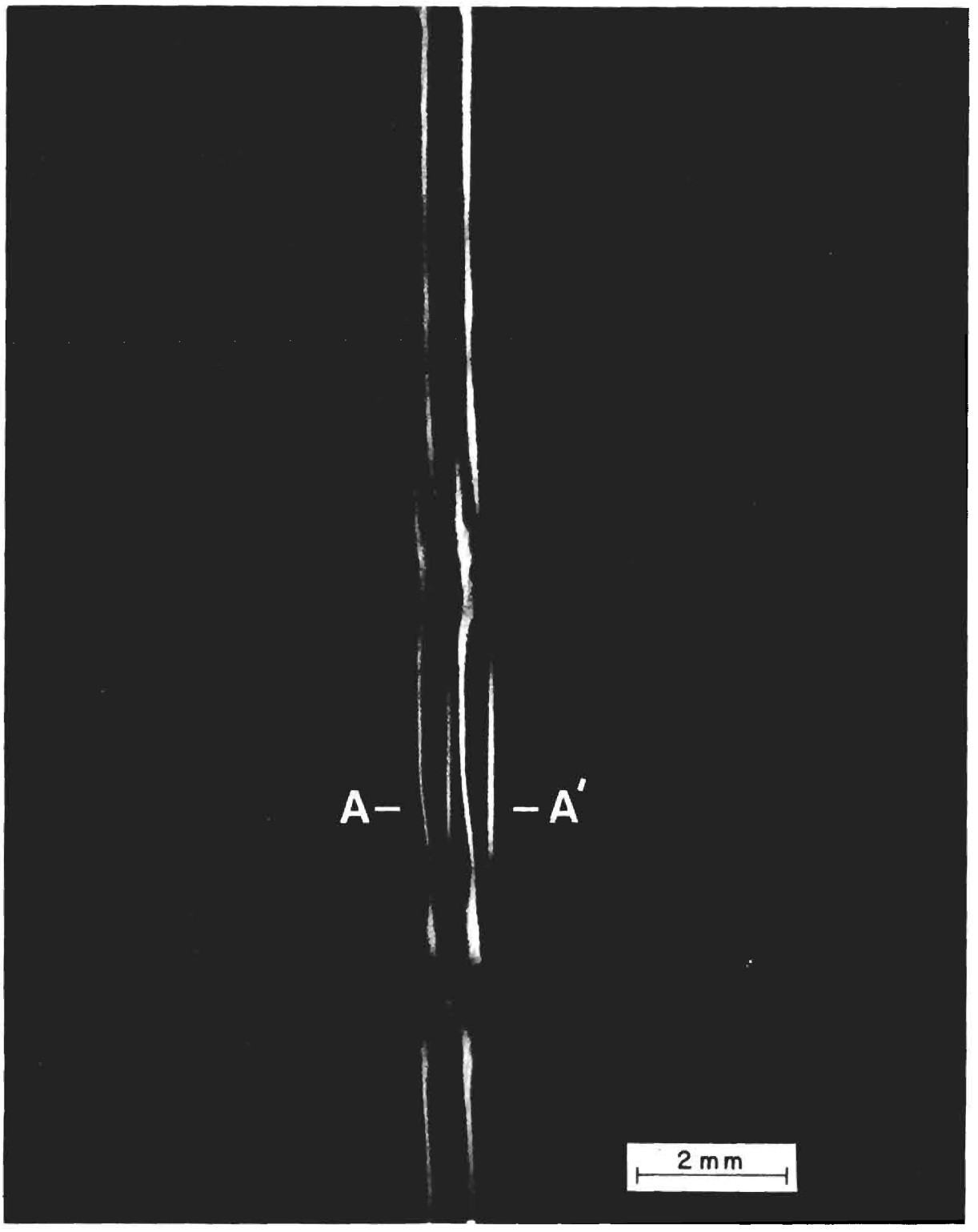

Figure 14.

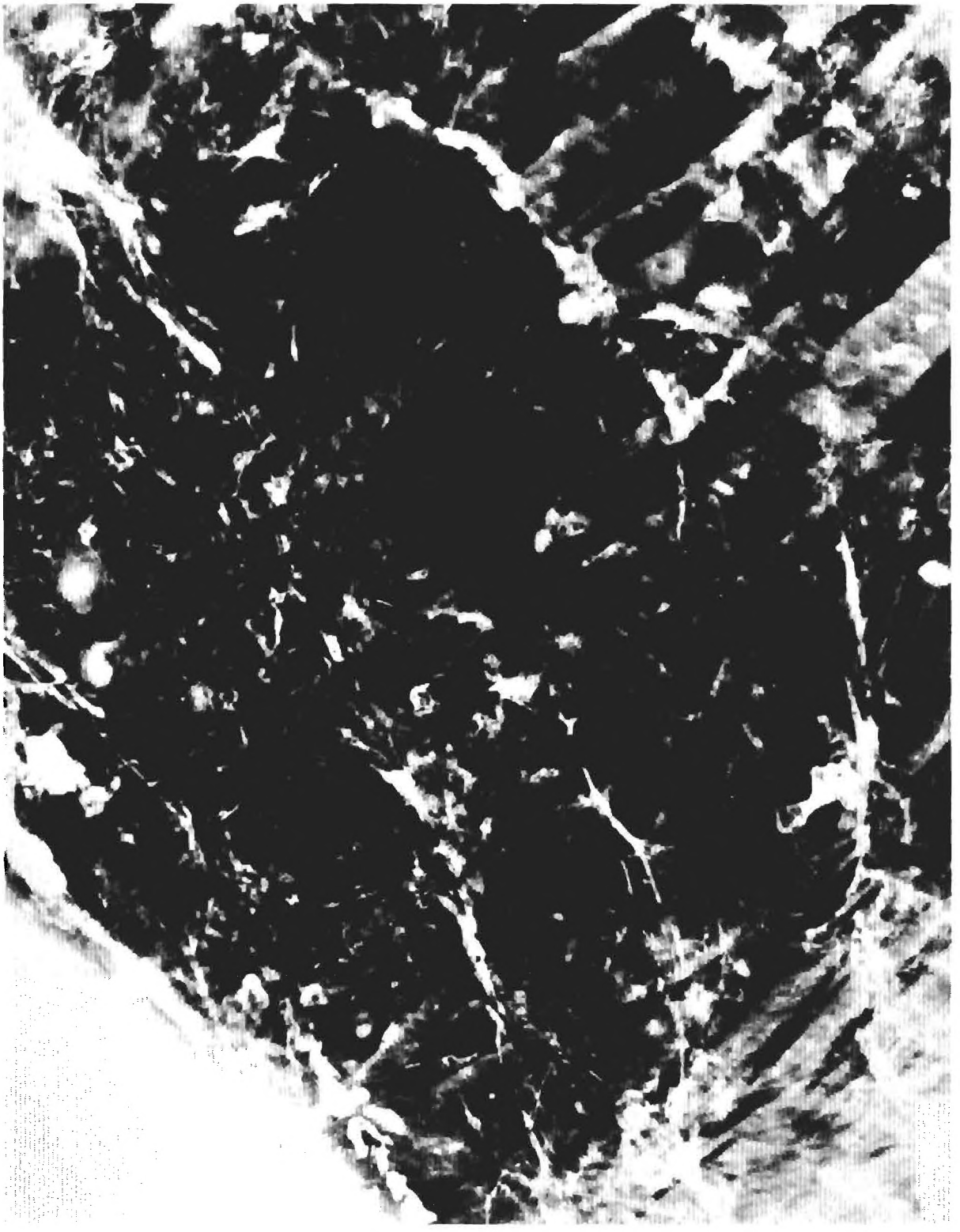

Figure 15.

APPENDIX II

Presentations and a manuscript relating to features in tourmaline (elbaite) R6538 (Smithsonian)

1. Pollard, C.O., Jr., and C. E. Wagner (1971) X-ray diffraction topographic and source-image distortion study of sector zoning in a tourmaline crystal (oral), Amer. Geophys. Union Conference on Petrologic Crystal Chemistry.
2. Pollard, C.O., Jr. and C. E. Wagner (1973) Strains associated with chemical boundaries in a sector-zoned Elbaite tourmaline crystal (Abstract), Geol. Soc. Amer., S.E. Section, Ann. Mtg. in Knoxville.
3. Pollard, C.O., Jr. and W.S. Parks, Jr. (1973) Strains associated with color boundaries in a sector-zoned tourmaline (elbaite) crystal (To be submitted).

STRAINS ASSOCIATED WITH COLOR BOUNDARIES IN A SECTOR-ZONED TOURMALINE (ELBAITE) CRYSTAL

Charles O. Pollard, Jr.
School of Geophysical Sciences
Georgia Institute of Technology
Atlanta, Georgia 30332

and

W. Scott Parks, Jr.
School of Geophysical Sciences
Georgia Institute of Technology
Atlanta, Georgia 30332

ABSTRACT

The color zones of the elbaite crystal R6538 (Smithsonian) lie in a sectorial pattern; however, microprobe and visible-light spectrophotometric results indicate that the two types of sectors are essentially the same chemically (with the slightly possible exception of Al_2O_3 and SiO_2). Basal plates of the crystal are light green in the first-order prism sectors and dark green in the second-order prism sectors. No measurable cell-parameter differences across sector boundaries have been detected. Rotational misorientations are measurable at some of the sector boundaries, each involving a rotation of less than 40 seconds of arc around an axis parallel to the boundary normal. These rotational misorientations can be measured on boundaries that are roughly parallel to second-order prism faces, separating sectors behind first and second-order prism faces. The basal component of the fault vector characteristic of any particular sector boundary is observed to lie normal to the boundary for all the fault vectors whose orientations could be determined. Only one boundary (roughly parallel to a first-order prism face and separating sectors behind first and second-order prism faces) was describable purely by a fault vector, with no rotational misorientation.

Striae are found within the sectors (in x-ray diffraction SID patterns and Lang topographs) that indicate that the optical sectoring of R6538 is due to different scattering interactions between light and domains of different shapes in the two types of sectors. The domains are apparently linear or cylindrical in the dark-green sectors and lamellar in the light-green sectors. Those in the dark-green sectors are apparently elongated roughly along the c-axis direction and those in the light-green sectors are apparently oriented so that the c-axis direction lies roughly in the lamellae. These domains may correspond to the twinning domains recently proposed by Tsang and Ghose [1973].

INTRODUCTION

Several microprobe studies recently have illustrated anew the complexity of zoning in mineral grains. We refer mainly to the studies of sector-zoning, which happen to have been conducted on staurolite and pyroxene crystals [Hollister and Bence, 1967; Hollister and Hargraves, 1970; and Hollister et al., 1971]. Dollase and Hollister [1969] have discussed evidence as well for cation ordering differences between sectors in staurolite. Hollister [1970] has presented a model for the causes of sector-zoning in staurolite, based on interrelations among chemical equilibria from face to face, rates of growth, and rates of diffusion of growth material. Preston [1966], Strong [1969], and Hollister and Gancarz [1971] have discussed the origin of sector-zoning in clinopyroxenes.

Sector-zoning has not previously been documented as well in tourmaline, though it was considered and discarded as a possible explanation for the fine-scale lamellar features Wagner et al. [1971] described in the overgrowths of growth-zoned tourmalines. The lamellae they described had approximately the correct dimensions and were oriented correctly to have possibly been formed by sector-zoned behind alternate first-order and second-order prism faces that "oscillate" in the common oscillatory striations of tourmaline crystals. Probe traces run across the lamellar boundaries demonstrated a lack of sector-zoning involving substantial chemical differences. The sector-zoning of the new tourmaline crystal, which is described below, involves differences of color intensity between first-order and second-order prism sectors.

Several questions are raised by these examples of sector zoning, as well as by the common examples of growth zoning. First, by what mechanisms do zoned crystals accommodate the structural mismatches at zone boundaries? We have found [Wagner, et al., 1971] that zones can be broken up into orientational

domains, so the mismatches can not always be represented simply by differences in unit cell parameters or by discrete average orientations on each side of the zone boundary. Second, how can we measure quantitatively these mismatches and the strains associated with them? In order to delineate quantitatively some of the imperfections that make up, or are associated with, sector-zoning in a particular tourmaline crystal, we have used several techniques that are loosely grouped under the term "x-ray diffraction topography." These techniques supplement optical and chemical (e.g., microprobe) techniques, as is illustrated in the following discussion.

EXPERIMENTAL BACKGROUND

Specimen Material

The particular portion of a tourmaline crystal used in this study came from the Smithsonian U.S. National Museum collection, where it is catalogued as R6538. The portion we obtained was 2 cm high (parallel to c-axis), 4 cm wide, and 3 cm thick. The crystal had been sampled earlier, but no data from the earlier sampling have been brought to the attention of Dr. George Switzer [personal communication, 1971], who supplied the sample to us. A portion approximating the same size as ours remains in the museum.

The crystal is visibly sector-zoned, showing alternating prismatic light-green sectors and dark-green sectors. The sectors are visible when viewed down the c-axis of basal sections thinner than about 3 mm. A thin pea-green overgrowth rim surrounding the crystal is also visible in these basal sections. All the data presented here are from two, approximately 0.5 mm thick, sections of our portion of the crystal: one, R6538-4, is cut parallel to (00.1) and the other, R6538-7, is cut parallel to (01.0). Other basal cuts yield information in agreement with that reported below. The sections were polished with graded diamond paste compounds down to the 1 micron grade, then etched for 1

hour in a saturated aqueous solution of NH_4FHF to remove polishing damage.

Techniques

X-ray diffraction. The x-ray diffraction topographic and allied techniques that were used have all been described elsewhere, so they will be described only briefly here.

A single-source source-image distortion (SID) pattern [Young and Wagner, 1966; Wagner et al., 1971] is formed when a spot x-ray source is allowed to irradiate a surface or thin slab (depending on whether the diffraction geometry is for reflection or transmission, respectively) so that chosen Bragg planes are in diffracting position for a chosen characteristic wavelength of x-rays. An image of the source is formed on a film placed in the diffracted beam and is modified by imperfections in the actively diffracting portions of the crystal. This image arises from a band extending across the crystal. For a perfect crystal, the band is defined by the intersections of those portions of the Bragg planes contained in the crystal sample with a right circular cone, nominally with a cone angle that is the complement of the Bragg angle θ, and oriented such that the cone axis passes through the source spot and is normal to the Bragg planes. Even for a perfect crystal, the band in the image has a width determined by the rocking curve of the crystal, the spread of wave-lengths in the source, the angle between the Bragg planes and the surface of the crystal, and the width of the source. In an image from an imperfect crystal, the band exhibits variations in intensity and deflections in trend that give information about the imperfections at corresponding positions within the actively diffracting band on the crystal.

For a relatively perfect crystal a single source might provide information from such a small area of the crystal that the imperfections become difficult

to relate spatially to each other. Such was the situation with R6538. This difficulty has been dealt with in two ways in the present study. First, a series of additional spot x-ray sources have been stacked along a line. This process yields a multi-source SID pattern, which is equivalent to a composite of many single-source SID patterns. Second, the Lang topographic technique [Lang, 1959] has been used, in which the crystal is set up as in the single-source SID experiment, but the crystal and film are translated until the diffracting band has crossed the crystal an integral number of times. In the Lang technique, the incident beam is collimated by divergence slits so that the crossfire angle is considerably less than that allowed in the single-source SID technique.

Each of the three x-ray techniques described above is useful for answering particular questions. The more familiar Lang technique is most useful in determining the anisotropy in local strain. For example, by comparing Lang topographs of the same area taken with differing Bragg reflections, one can determine the location of a dislocation and the direction of the associated Burgers vector. The multi-source SID technique can provide the same topographic information but usually with less resolution; however, this technique can also yield quantitative measures of lattice misorientations and/or d-spacing differences between neighboring portions of a crystal (as from each side of a growth-zone boundary). The single-source SID technique may be required as a supplement to obtain this type of information when the neighboring bands in a multi-source SID pattern interfere with each other.

Electron Microprobe. The explanation for the color-intensity differences between the light-green and the dark-green sectors of R6538 was sought in electron microprobe chemical analyses of these parts of the crystal. The probe analyses

were carried out on another basal section which had virtually the same geometry of sectors and which was originally located approximately one and a half cm. away from R6538-4. The data were collected on an ARL microprobe run at 15 KV, and were visually monitored for assurance that the chemistry was relatively uniform within each of the standards and within each distinct portion of the sample. The standards are on file at the Department of Geology, University of Georgia. Garnet 12442 was used as a standard for SiO_2, Al_2O_3, and MgO. Aenigmatite was used as a standard for TiO_2 (total titanium), FeO (total iron), and MnO (total manganese). Amphibole 227 was used as a standard for Na_2O, K_2O, and CaO. The chemical analysis was not complete, in the sense that other known or possible components of tourmaline were not determined: boron, lithium, fluorine, hydroxyl, and water. Other potential trace elements were sought, but not detected: chromium, zinc, copper, and lead.

Visible-light spectrophotometry. Visible-light absorption spectrophotometry was utilized to characterize the details of the color spectrum and to seek differences in spectra from the two types of sectors. The spectrophotometer was a Beckman Acta 5 model. The portion of the spectrum that was studied lay between 12,000cm^{-1} and 30,000cm^{-1}.

RESULTS

Geometry of Sectors

Figure 1 shows a drawing of R6538-4, the most useful basal section of the crystal, with the sectors sketched in and labeled. It is presumed that the material in each sector has been added by growth on prism faces because other basal sections show the same configuration of sectors. The sectors are named for their growth faces and thus are idenfitied by the orientation of growth surfaces on or within the crystal. The relationship between R6538-4 and R6538-7, the

most useful prismatic section, is also shown in Figure 1 (R6538-7 joined R6538-4 along the line A-A'). R6538-7 was cut from a volume of crystal adjacent to R6538-4 and its limiting cuts were oriented normal to those of R6538-4. Boundaries to be discussed later are numbered as well in Figure 1.

Figure 2 is a $(\bar{4}\bar{4}.0)$ transmission Lang topograph of the basal section, R6538-4. Besides the final growth horizon or crystal outline, the growth horizons labeled a-b, b-c, a-d, e-f and g-h in Figure 2 could be identified in this basal section. Four $(2\bar{1}.0)$ horizons, two (10.0) horizons, two $(\bar{1}\bar{1}.0)$ horizons, and two $(\bar{2}1.0)$ horizons have been detected in topographs from a fragmented basal section that was separated from R6538-4 by 5mm. That we could not identify earlier crystal outlines in the other two sectors obviously reduces the trustworthiness of our assignment of a particular Miller-Bravais symbol to the complete volume of each of those sectors. The configuration of sectors illustrated in Figure 1 is hence the most reasonable model developed. However, growth on additional faces may have occurred locally within any of the indicated sectors. In this interpretation, the color differences among prismatic sectors are such that growth material incorporated via first-order prism faces is lighter green than material in second-order prism sectors.

The thin pea-green overgrowth rim has obscured the final prism faces for the sectors under discussion. Before growth of the rim, fine-scale alternation of first and second order prisms, which forms oscillatory striations, apparently had/not occurred. Such oscillatory striations are, however, evident on the outer boundary of the pea-green rim, the edges of the basal section.

Chemical Results

The partial electron microprobe analysis results are given in Table 1. Within each of the two types of sector zones (light-green and dark-green), the crystal was revealed to be chemically homogeneous by reasonable repetition of

the counting rates at several sites. The errors indicated in Table 1 are standard counting-rate errors. Only for SiO_2 and Al_2O_3 (the two oxides with the highest counting rates) did the most errant counting rates differ from the mean by more than three counting-rate standard deviations. For Al_2O_3 and SiO_2, the worst deviations from the means were about five times the counting-rate standard deviations; however, simultaneous detection of the same oxide in two channels for each of Al_2O_3 and SiO_2 showed that these deviations were most probably instrumental fluctuations rather than spatial inhomogeneities in Al_2O_3 and SiO_2 content within each type of sector.

As shown in Table 1, the compositions of the light and the dark sectors were surprisingly similar for those oxides that could be detected. The differences between types of sectors for Al_2O_3 and SiO_2 are the only ones that exceed the counting-rate errors. In view of the greater fluctuations in actual counting-rates for Al_2O_3 and SiO_2, it is doubtful that these differences are significant.

Optical Results

The visible-light spectra looked similar to published spectra for green tourmaline; spectra for both the extraordinary and ordinary rays are essentially equivalent to those of Faye et al. [1968] and Wilkens et al. [1969] with broad peaks centered at 14,000 cm^{-1} and 24,000 cm^{-1}. E⊥c (ordinary ray) spectra could easily be obtained from the two distinctly colored regions of R6538-4, the basal section. The E⊥c spectra of the dark green sectors were similar to E⊥c spectra of the light green sectors, but the absorbance was approximately 10% greater at each wave-length in the dark sectors.

Masking of light green sectors from dark green sectors (and vice versa) was not accomplished when spectra were obtained from R6538-7, the smaller and thinner prismatic section. Consequently no difference was detected between

the E||c spectra from the two types of sectors. In fact, boundaries 3 and 5, which are so obvious in light transmitted through R6538-4 and other basal sections, can not be found in R6538-7 by polarized light. Whether the light is polarized with E||c or with E⊥c or in a general direction, the boundaries can not be perceived. Obviously, whatever causes the apparent color zoning in the basal sections is more sensitive to direction of propogation of transmitted light than to its polarization direction. Interpretation of these puzzling observations will be deferred until after necessary x-ray observations are presented.

Sector Boundaries-Basal Section

By comparing Lang topographs made with several Bragg reflections, anisotropy of strain associated with sector boundaries could be characterized; however, this information, plus quantitative measures of lattice misorientations and/or parameter changes across sector boundaries was actually obtained from SID patterns of R6538-4. The rationale involved in characterizing strains stored at sector boundaries will be demonstrated by analyses of multi-slit SID patterns for two types of boundaries; the findings for some of the other types of sector boundaries found in R6538-4 will be compiled in a table. The boundaries to be discussed are as follows: (1) the boundary that is roughly parallel to (10.0) and is between the ($2\bar{1}$.0) and the ($\bar{1}$0.0) sectors, and (2) the two boundaries that are roughly parallel to ($\bar{1}$2.0) and are between the ($2\bar{1}$.0) and (10.0) sectors. These three boundaries are labeled respectively 1, 2, and 3 in Figure 1.

Figure 3a is a ($\bar{2}$4.0) transmission multi-source SID pattern. Figure 3b is a (30.0) transmission multi-source SID pattern. Because the image is distorted somewhat, maps of the features shown in each pattern are provided in Figures 3c and 3d. The boundaries under discussion (1, 2, and 3) can be located by referring to Figures 1 and 3. Boundary 1 is extinct (missing) in Figure 3a; i.e., there is no charge in intensity or offset in the SID bands where we know the boundary

to be. Boundaries 2 and 3 are readily apparent in Figure 3a; the SID lines that run down the portion of the image corresponding to these boundaries are considerably more intense than neighboring SID lines. In Figure 3b, boundary 1 is evident because of the intensity contrast in the SID lines running down each side of the boundary. Also in Figure 3b, boundaries 2 and 3 are now not quite extinct intensity-wise and measurable offset of each SID line exists at each of these two boundaries.

If a crystalline imperfection has associated with it anisotropic strain describable by a localized fault (displacement) vector $\vec{f}$ in the direction of the displacement, the orientation of $\vec{f}$ can be determined by analysing the extinction behavior of the imperfection in topographic and SID images. The condition for extinction is $\vec{f} \cdot \vec{H}(hk\ell) = 0$, where $\vec{H}(hk\ell)$ is the reciprocal lattice vector to reciprocal lattice point $hk\ell$, which corresponds to the diffraction vector during Bragg diffraction. Thus if minimum contrast for a feature is observed for reflection from a particular set of planes $(hk\ell)$, the fault vector associated with that feature must lie in a plane normal to the reciprocal lattice vector $\vec{H}(hk\ell)$ (i.e. parallel to the diffracting Bragg planes).

On the basis of the two patterns shown here, Figures 3a and 3b, it is demonstrated that the fault vectors involved in boundary 1 lie in planes of the group $(\bar{1}2\cdot\ell)$; i.e., the vectors must lie in one of the group of planes which share the same intersection line on the basal section with the active Bragg planes in Figure 3a, $(\bar{2}4.0)$. The ℓ-index is required by the space group to be an integral multiple of 3. Other patterns, of lower quality than those shown but nevertheless diagnostic, demonstrate when one of these reflections with a multiple of ℓ other than zero is used, the contrast at boundary 1 becomes enhanced. This shows that the c-axis components of the fault vectors associated with boundary 1 lie in $(\bar{1}2.0)$. Figure 3a and 3b demonstrate directly, without other evidence, that the components of $\vec{f}$ in the basal plane lie in $(\bar{1}2.0)$, the planes containing the c-axis and normal to the boundary. Therefore, according to the extinction condition, boundary

1 in Figure 3 involves faults describable by fault vectors that lie in $(\bar{1}2.0)$.

The absence of off-set in the SID lines at boundary 1 is informative in a different respect. For the SID lines to cross such a boundary in a $(hk\cdot\ell)$ SID pattern without deflection proves that the only possible axis of rotational mismatch is parallel to the $\vec{H}(hk\cdot\ell)$ reciprocal lattice vector (i.e., the active Bragg planes are parallel on both sides of the boundary) and that the d-spacing of the $(hk\cdot\ell)$ planes is the same on both sides of the boundary. In fact, no offset in SID lines was detected at boundary 1 in any SID pattern, no matter which reflection was used.

Analyzed in light of the extinction condition, boundaries 2 and 3 are shown to involve faults whose fault vectors lie in (10.0); however, additional mismatch factors are also involved in these boundaries. All possible reflections have not been used to obtain SID patterns, but the best interpretation of our data is that boundaries 2 and 3 can not be made to become completely extinct. The strongest argument for this view is that Figure 3b shows these boundaries in minimum contrast and that they increase in contrast for neighboring reflections for which they should logically decrease in contrast if they could ever be extinguished.

The simplest explanation for the remaining contrast in Figure 3b, the pattern with minimum contrast for these boundaries, is suggested by the offset in the SID lines as they cross boundaries 2 and 3. The offset in SID lines seen on boundaries 2 and 3 in Figure 3b is the maximum offset detected in any SID pattern. The offset is diagnostic of either a misorientation or a d-spacing change. The difference between these two possibilities can be determined in general by obtaining two patterns using different orders of the same reflection. At each point, the shift of the diffracting band from its nominal position is determined by the component of tilt about an axis lying in the active Bragg planes or by a change in spacing of the active Bragg planes, or by a combination

of both. The angular change produced by a strain, $\frac{\Delta d}{d}$, increases with the tangent of the Bragg angle, whereas the angular change produced by a tilt is independent of the Bragg angle. The contributions of tilt and strain to the distortion of the image can, therefore, be separately determined from observations made with two or more orders of the same reflection. If the mismatch is shown to be purely rotational (involves no d-spacing change), ideal SID patterns can reveal the orientation of the axis of the rotation within the Bragg plane. The sensitivity to magnitude of rotation shown in off-sets of SID lines decreases from highly sensitive for rotation about the axis normal to the plane of incidence to relatively insensitive for rotation about the axis defined by the intersection of the Bragg planes with the plane of incidence. Moreover, components of rotations about the direction normal to the plane of incidence cause no redirection in trend of the SID lines on one side of the boundary relative to the trend on the other side; redirection of SID lines is observed for components of rotation about the axis lying in the plane of incidence and the Bragg plane. A significant segment of the SID band must be unaffected by other deflecting features for this criterion to allow total separation of components of rotation about the axes within the Bragg planes.

In this particular instance, the choices were narrowed by obtaining a pattern similar to Figure 3b using the (60.0) reflection. No redirection in SID line trend is observed in either pattern and the offset is not dependent on the Bragg angle. The principal cause of the offset is therefore misorientation across the boundaries. The lattice on one side is rotated with a rotational component about an axis parallel to $\vec{H}(\bar{1}2.0)$ by approximately 40 seconds of arc. This amount of rotation is arrived at by a simple geometric calculation, considering the offset of the SID lines and instrumental dimensions.

The other boundaries for which we have data that could be analyzed in similar fashion are labeled 4 and 5 in Figure 1. The data from all five boundaries are

given in Table 2. Boundary 1 is the only one that involves simply faulting mismatches; the other boundaries involve also rotational mismatches. None of the boundaries studied involve d-spacing changes. The orientations of the fault vectors are characterized as well as possible. Separate mismatches, those describable by rotation about axes normal to the respective boundaries, are given for four boundaries. The magnitudes of these rotations were calculated in each instance by accounting for the amount of SID-line off-set relative to the geometrical dimensions during the experiments.

Prismatic Section

All of the results from R6538-7, the prismatic section, do not correlate completely with results discussed above from the basal section. Figure 4 is a collection of patterns showing R6538-7: Figure 4a is a (00.3) Lang transmission topograph, Figure 4b is a (30.0) Lang transmission topograph, Figure 4c is a (00.3) multi-source transmission SID pattern, and Figure 4d is a (30.0) multi-source transmission SID pattern. Boundaries 3 and 5 are correlated from pattern to pattern. The dark-green sectors are at either end and are more heavily striated than the light-green sectors, with the general trend of the striae running parallel to the c-axis. From left to right, the section passes through the sectors in the following order: $(2\bar{1}.0)$, (10.0), $(\bar{1}0.0)$, and $(\bar{2}1.0)$. The sector boundary between the two light green sectors (10.0) and $(\bar{1}0.0)$ is not detectable, but the boundaries of these with the dark-green $(2\bar{1}.0)$ and $(\bar{2}1.0)$ sectors on each side (boundaries 3 and 5) can be detected.

Boundary 3 is perceptible in all four patterns of Figure 4; however, boundary 5 is less apparent in Figure 4b, the Lang topograph made with the (30.0) reflection (that portion of the crystal is not imaged in Figure 4d, the corresponding SID pattern). For both boundaries, the boundary is recognizable because of a change in the nature of the features in the adjacent sectors, rather than intensity contrast attributable to the boundary itself.

Part of the difficulty with identifying features in R6538-7 and correlating them with features in the basal section is the background clutter in all the patterns, a feature of R6538-7 that could not be improved. Additional etching did not improve it, so surface damage does not explain the clutter.

The most positive correlation between the basal plate and R6538-7 is found at boundary 3. The boundary involves offsets in the (00.3) SID lines in Figure 4c, indicating that there is a d-spacing change or a component of rotation about some axis in the basal plane in the mismatch at boundary 3. If the boundary were isolated from other features that deflect the SID lines, it would be possible to distinguish between d-spacing change and tilt or, if it is purely a tilt, to characterize the direction of the axis of rotation within the Bragg plane further; however, the striae also deflect the SID lines. Hence, no "baseline" for comparison of trends from one sector to the other is available. Further restriction in the components of rotational mismatch has not been possible with other patterns from R6538-7, for the same reason. Nevertheless, the offsets in SID lines at boundary 3 in Figure 4c is consistent with the characterization of mismatch factors determined at boundary 3 in Figure 3. Considering all the other data from R6538, it is unlikely that d-spacing changes are involved at boundaries 3 and 5.

Strains not at Boundaries

It is outside the purpose of this paper to analyze fully the striae seen within the sectors, but these features are unreported and may explain some of the discrepancies in the optical and chemical data. The striae in the light green sectors can be seen in Figure 2 just below boundaries 1 and 4, and between boundaries 2 and 3./ Other topographs of the basal section show striae also in the $(0\bar{1}.0)$ light green sector . No striae were seen in the dark green sectors of the basal slice, no matter the reflection that was used. The striae were sought in Lang topographs of R6538-4 taken in reflection geometry [(00.3) and (00.6) reflections], but were not found. Reflection topographs are more subject to degradation of quality by

surface damage and scratches, so this observation is less trustworthy than the positive observation of the striae with non-basal reflections. Occasionally of R6538-7
SID lines/are seen to be off-set by the striae, but no way has been found to correlate a particular stria from pattern to pattern; therefore, it has not been possible to distinguish from the SID patterns between d-spacing changes and lattice rotations as causative mechanisms.

Striae of different characteristics are found in patterns of R6538-7. One set of striae is found in the dark-green sectors and is seen best in Figure 4a to the outsides of boundaries 3 and 5. The other set of striae is found in the light-green sectors to the inside of boundaries 3 and 5 in Figure 4a; the striae in this second set are significantly more sparce than those in the dark-green sectors. The striae are visible as lines of offsets in SID lines in Figure 4c and as splitting of SID lines in Figure 4d. Since these striae are not the principal feature of interest here they have not been fully characterized, but it can be said from the SID patterns that, if they involve only rotational mismatches, there is a large component of that rotation about the $\bar{1}2.0$ reciprocal lattice vector. If, on the other hand, they involve only d-spacing changes, then both a- and c-cell parameters are affected.

The striae in the dark green sectors of R6538-7 have not been identified in the patterns from R6538-4. The most likely explanation for their absence in R6538-4 is that they are linear or cylindrical features with their elongated direction along the c-axis, so that they would be difficult to recognize in R6538-4. The striae in the light-green sectors of R6538-7 are thought to correlate with those in the light-green sectors of R6538-4. If this interpretation is correct, the striae in the light-green sectors represent the intersection of lamellar features (oriented roughly parallel to the c-axis) with the plane of each section.

DISCUSSION

The microprobe results reveal that there is essentially no difference in the chemistry (with the possible exceptions of Al_2O_3 and SiO_2) between light-green and dark-green sectors of R6538. [In a sense, the crystal is therefore not sector-zoned; however, no alternative term exists yet for crystals that are color-zoned in sectorial pattern without chemical sector-zoning.] The optical results also indicate that there is little or no chemical difference between types of sectors. The types of sectors can not be distinguished in the prismatic section, even in light transmitted with E⊥c. The transmission spectrum from light-green sectors in the basal section could be interpreted as representing dilution of the same absorbing species in the same ratio as found in the dark-green sectors; however, a more reasonable interpretation, in view of all the spectra, is that light is scattered differently in the two types of sectors for light transmitted through the basal section but not for light transmitted through the prismatic section. The most reasonable explanation for the observed optical interactions is that the absorbance shown in the spectra is dependent not only on polarization, but also on the geometric relationship of the scattering features to the propagation direction of the light. The differential scattering is apparently not too sensitive to optical wavelength, so the effect of a smaller scattering interaction on the spectra is similar to a dilution effect.

The features in the x-ray patterns that most likely correspond to the proposed scattering features are the striae within the sectors. These striae apparently have the three-dimensional shapes to interact with light in the required manner. The striae in the dark-green sectors are definitely not lamellae similar to those found in overgrown tourmalines by Wagner et al. [1971]; they can not be correlated from the basal to the prismatic sections, so they are most likely cylindrical or linear features that are elongated roughly parallel to the c-axis in the dark-green

sectors. The striae in the light-green sectors could well correspond to the lamellae found in overgrown tourmalines, as they apparently represent the intersection of tabular features with the planes of each section. The scattering features thus would appear essentially the same in both types of sectors in the prismatic section, but quite different in the two types of sectors in the basal section; these are the requirements that must be met to explain the optical behavior. The striae are spaced at about 0.03mm in the topographs with the best resolution. Hence the nature of the scattering interactions would not seem to be related to the Schiller effect or to form birefringence effects, unless there are finer striae smaller than our level of resolution.

In discussing the weak and broad satellite signals they obtained during NMR studies of an elbaite crystal, Tsang and Ghose [1973] suggested the presence of fine-scale twinned domains. Our results do not necessarily corroborate this suggestion, but the explanation for the apparent differential scattering behavior of R6538 may lie in the different orientations of the boundaries of such domains. In fact, the striae that are obvious in x-ray patterns from R6538 may represent the strain fields from the interfaces among such domains. In order to fully characterize such striae in tourmaline by x-ray topography, less dense spacing of the striae will be necessary. Transmission electron microscopy will be necessary to characterize striae as close-spaced as those in R6538.

The strains associated with the sector boundaries, measured quantitatively on boundaries 1 through 5, must represent the mismatches that occur at interfaces between material in which the domains (assuming the striae represent Tsang-Ghose twinning domains) are elongated on one side of each boundary and planar on the other side. Since these different shapes were established during growth (behind different faces), presumably at elevated temperature, the strains reported here may not have been present at the time of growth. Differential contractions after growth for differently shaped form-anisotropic volumes of material might explain the boundary strains.

ACKNOWLEDGEMENTS

This research was principally supported by the U.S. Army Research Office - Durham. Acknowledgement is also made to the donors of The Petroleum Research Fund, administered by the American Chemical Society, for partial support of Pollard. The efforts of J. Conrad Meaders are appreciated, for his conduction of some of the SID experiments. John C. Stormer, Jr., aided in the conduction of the electron probe analysis. George Switzer was helpful in arranging for our loan of the crystal material. An anonymous reviewer of an earlier version of this manuscript made helpful suggestions for the graphical presentation of the data. We thank C. E. Wagner for preliminary x-ray data and interpretations. Harry Hopkins helped by obtaining the visible-light spectra.

REFERENCES

Dollase, W.A., and L.S. Hollister, X-ray evidence of ordering differences between sectors of a single staurolite crystal, Discussion paper presented at the Geol. Soc. Amer. Atlantic City Meeting, 1969.

Faye, G.H., P.G. Manning, and E.H. Nickel, The polarized optical spectra of tourmaline, cordierite, chlorotoid, and vivianite, Amer. Mineral., 53, 1174-1201, 1968.

Hollister, L.S., Origin, mechanism, and consequences of compositional sector-zoning in staurolite, Amer. Mineral., 55, 742-766, 1970.

Hollister, L.S., and A.E. Bence, Staurolite: Sectoral compositional variations, Science, 158, 1053-1056, 1967.

Hollister, L.S., and R.B. Hargraves, Compositional zoning and its significance in pyroxenes from two coarse grained Apollo 11 samples, Proc. Apollo 11 Lunar Sci. Conf., Geochim. Cosmochim, Acta Suppl. 1, v. 1, 541-550, Pergamon, 1970.

Hollister, L.S., and A. J. Gancarz, Compositional sector-zoning in clinopyroxene from the Narce Area, Italy, Amer. Mineral., 56, 959-979, 1971.

Hollister, L.S., W. E. Trzcienski, Jr., R. B. Hargraves, and C. G. Kulick, Petrogenetic significance of pyroxenes in two Apollo 12 samples, Proc. Second Lunar Sci. Conf., v. 1, 529-557, MIT Press, 1971.

Lang, A. R., Studies of individual dislocations in crystals by x-ray diffraction microradiography, J. Appl. Phys., 30(11), 1748-1755, 1959.

Preston, J., An unusual hourglass structure in augite, Amer. Mineral., 51, 1227-1233, 1966.

Strong, D.F., Formation of the hour-glass structure in augite, Mineral. Mag., 37 (288), 472-479, 1969.

Tsang, T. and S. Ghose, Nuclear magnetic resonance of ^{1}H, ^{7}Li, ^{11}B, ^{23}Na, and ^{27}Al in tourmaline (elbaite), Amer. Mineral., 58, 224-229, 1973.

Wagner, C. E., C.O. Pollard, Jr., R.A. Young, and Gabrielle Donnay, Texture variations in color-zoned tourmaline crystals, Amer. Mineral., 56, 114-132, 1971.

Wilkens, R.W.T., E.F. Farrell, and C.S. Naiman, The crystal field spectra and dichroism of tourmaline, J. Phys. Chem. Solids, 30, 43-56, 1969.

Young, R.A., and C.E. Wagner, X-ray source-image distortion technique for the study of crystal distortion and vibration, J. Appl. Phys., 37(11), 4070-4076, 1966.

TABLE 1. Partial* Electron Probe Microanalyses

	Light-green Sectors	Dark-green Sectors	Counting Error
SiO	35.21	34.43	0.12
Al_2O_3	41.08	41.62	0.20
FeO (Total Fe)	5.95	5.99	0.12
Na_2O	2.90	2.92	0.06
MnO (Total Mn)	1.09	1.12	0.04
CaO	0.17	0.16	0.01
MgO	0.11	0.11	0.01
TiO_2 (Total Ti)	0.07	0.11	0.02
K_2O	0.04	0.05	0.01

*Not determined: Boron, lithium, fluorine, hydroxyl, water.

TABLE 2. Strains Stored at Sector-Zone Boundaries

Boundary (see Figure 1)	Sectors Involved	Approximate Indices of Boundary	Fault Vector $\parallel$ to (hkℓ) Planes	Misorientation by rotation around $\vec{H}$(hkℓ)	
				rotation angle (sec.)	rotation axis
1	$(2\bar{1}.0),(\bar{1}0.0)$	(10.0)	$(\bar{1}2.0)$	--	--
2 and 3	$(2\bar{1}.0),(10.0)$	$(\bar{1}2.0)$	(10.0)	40"	$\vec{H}(\bar{1}2.0)$
4	$(\bar{1}2.0),(\bar{1}0.0)$	(11.0)	$(1\bar{1}.0)$	25"	$\vec{H}(11.0)$
5	$(\bar{1}0.0),(\bar{2}1.0)$	(11.0)	$(1\bar{1}.0)$	20"	$\vec{H}(11.0)$

FIGURE LEGENDS

Fig. 1a. Drawing of the basal section of R6538 showing the surmised sectors, labeled boundaries for later discussion, and the intersection with R6538-7 along AA'.

1b. The vectors define our axial system for this paper; each vector is a reciprocal lattice vector, normal to the planes with the indicated indices.

1c. Idealized sector-zoned crystal. The shaded sectors would be dark-green if such an idealized crystal grew with the same type of zoning exhibited by R6538. Only the light-green, first-order prism sectors are labeled.

Fig. 2. Transmission ($\bar{4}\bar{4}$.0) Lang diffraction topograph of R6538-4 showing growth horizons a-b and e-f in the ($\bar{1}$2.0) sector, a-d in the (2$\bar{1}$.0) sector, b-c in the ($\bar{1}$0.0) sector, and g-h in the ($\bar{1}\bar{1}$.0) sector. The image is in negative contrast.

Fig. 3a. Multi-source SID pattern of R6538-4, made using the ($\bar{2}$4.0) reflection in the transmission geometry. Part of the image from another reflection is superimposed on the left portion of the image. The image is in negative contrast.

3b. Multi-source SID pattern of R6538-4, made using the (30.0) reflection in the transmission geometry. The image is in negative contrast.

3c. Map of features shown in Figure 3a, with the boundaries labeled as in Figure 1. The hachured region down and to the left of a line between the labels 4 and 5 is the superimposed image from another reflection.

3d. Map of features shown in Fig. 3b, with the boundaries labeled as in Figure 1.

Fig. 4. Four patterns of R6538-7. This slice joined R6538-4 in Figure 1 along the line A-A' so that the A' corner here was adjacent to the A' in Figure 1 and so that the top of the image joined R6538-4. The (2$\bar{1}$.0) sector is on the left and the ($\bar{2}$1.0) sector is on the right. Boundaries 3 and 5 are correlated among the patterns. All the images are in negative contrast.

4a. Transmission (00.3) Lang topograph

4b. Transmission (30.0) Lang topograph

4c. Transmission (00.3) multi-source SID pattern

4d. Transmission (30.0) multi-source SID pattern.

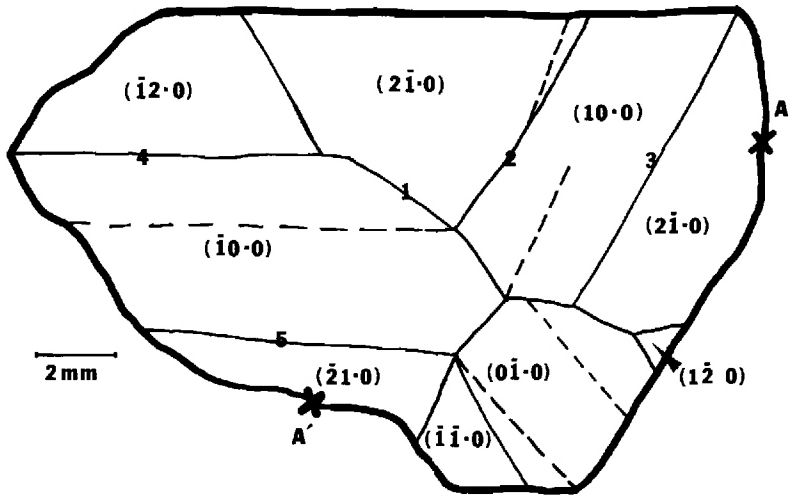
(ī2·0)
(2ī·0)
(10·0)
A
4
2
3
1
(ī0·0)
(2ī·0)
5
2mm
(2̄1·0)
(0ī·0)
(1ī 0)
A´
(īī·0)

1a

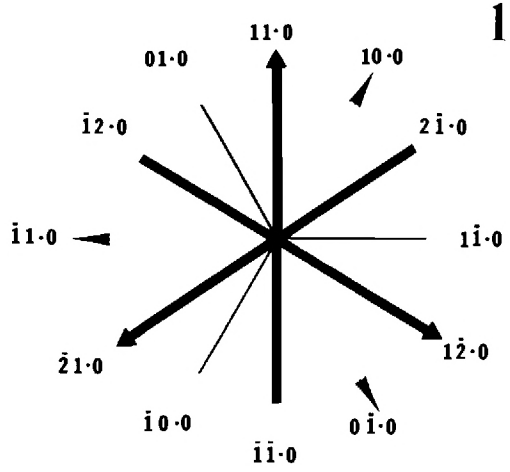
11·0
01·0
10·0
ī2·0
2ī·0
ī1·0
1ī·0
2̄1·0
1ī·0
ī0·0
0ī·0
īī·0

1b

1c

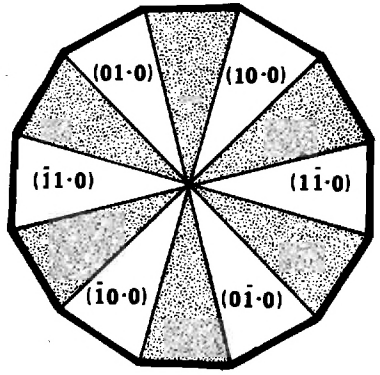
(01·0)
(10·0)
(ī1·0)
(1ī·0)
(ī0·0)
(0ī·0)

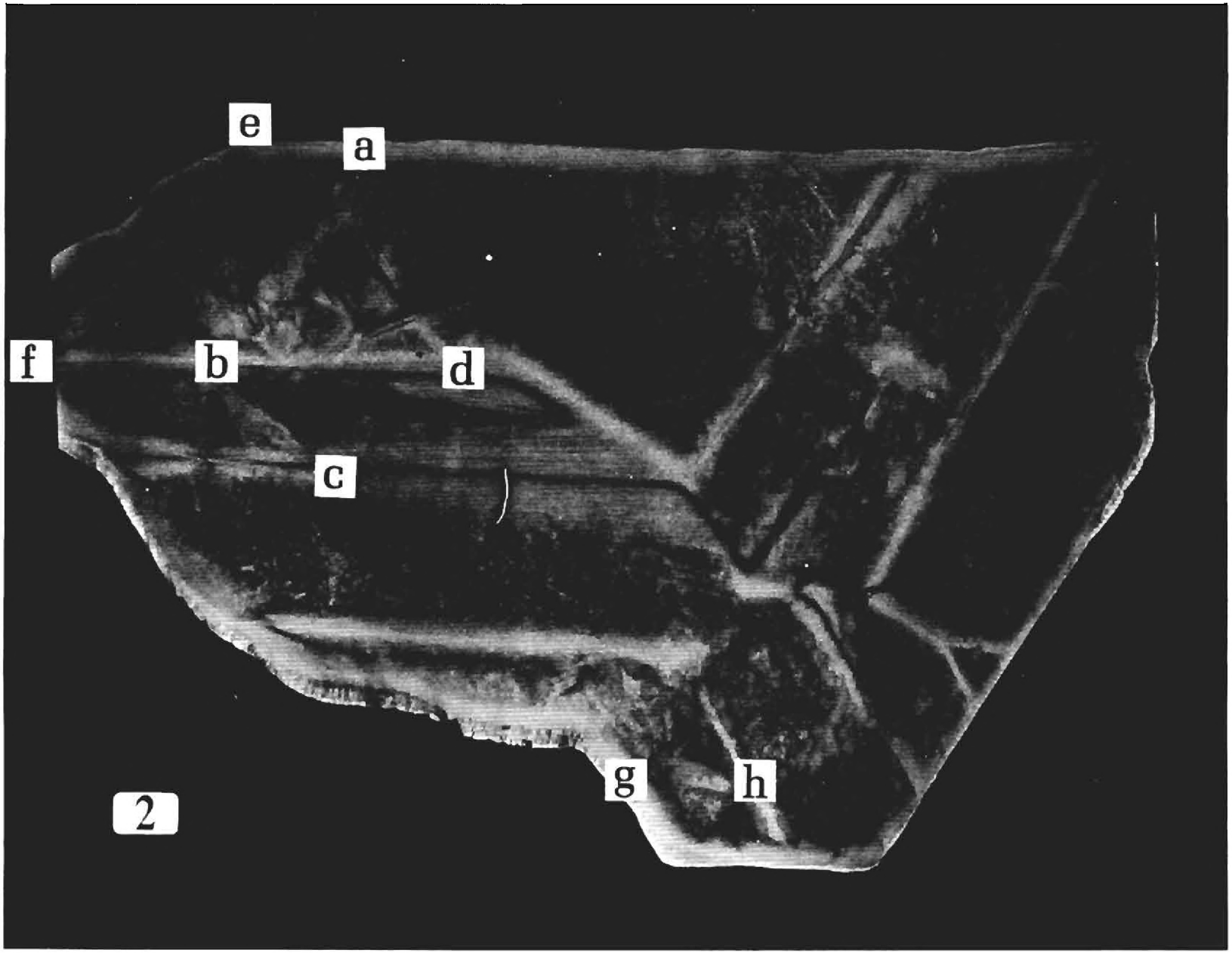
e
a
f
b
d
c
g
h
2

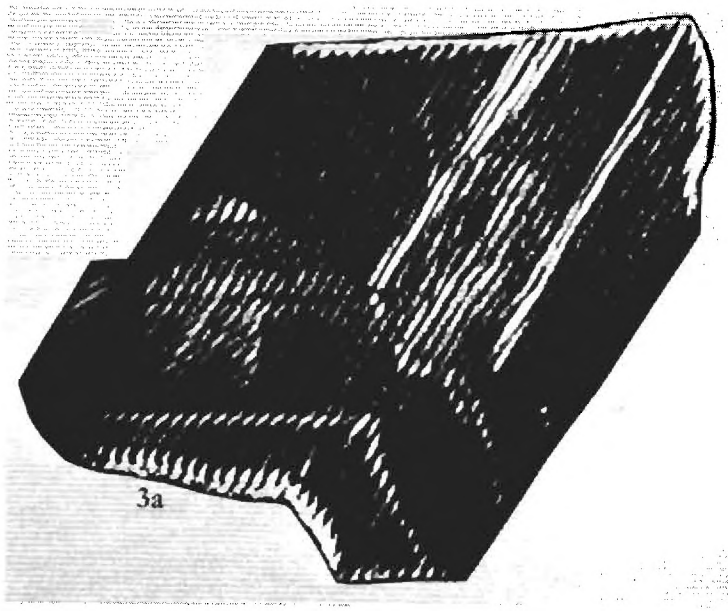

3a

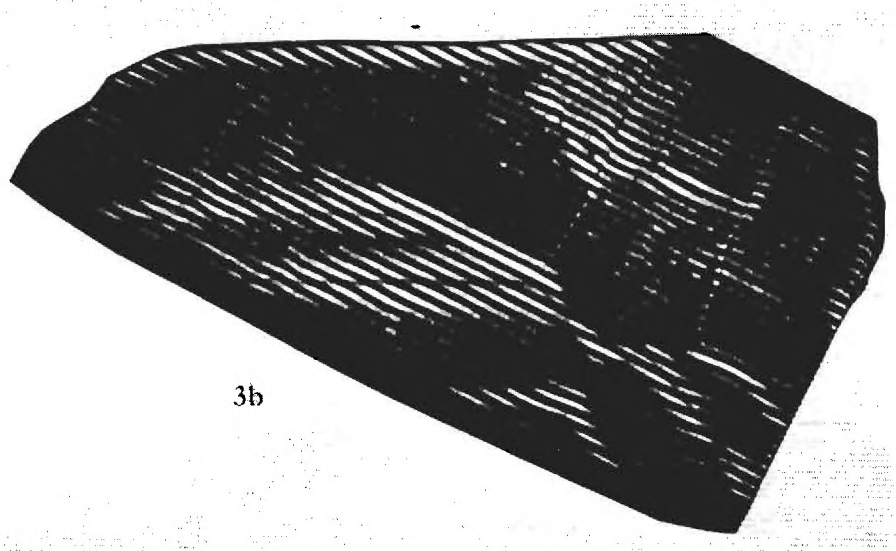

3b

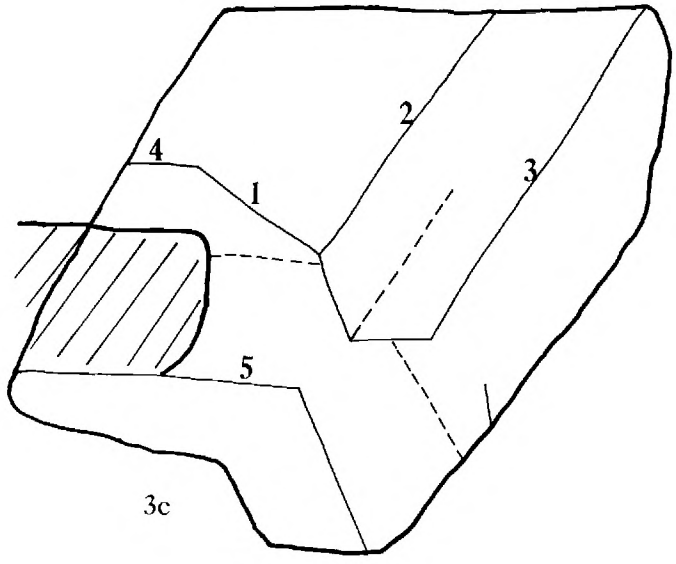

3c

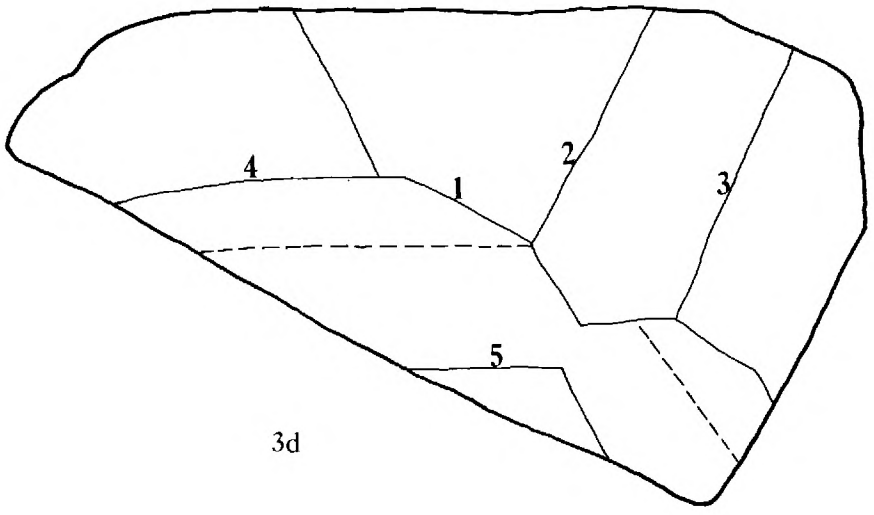

3d

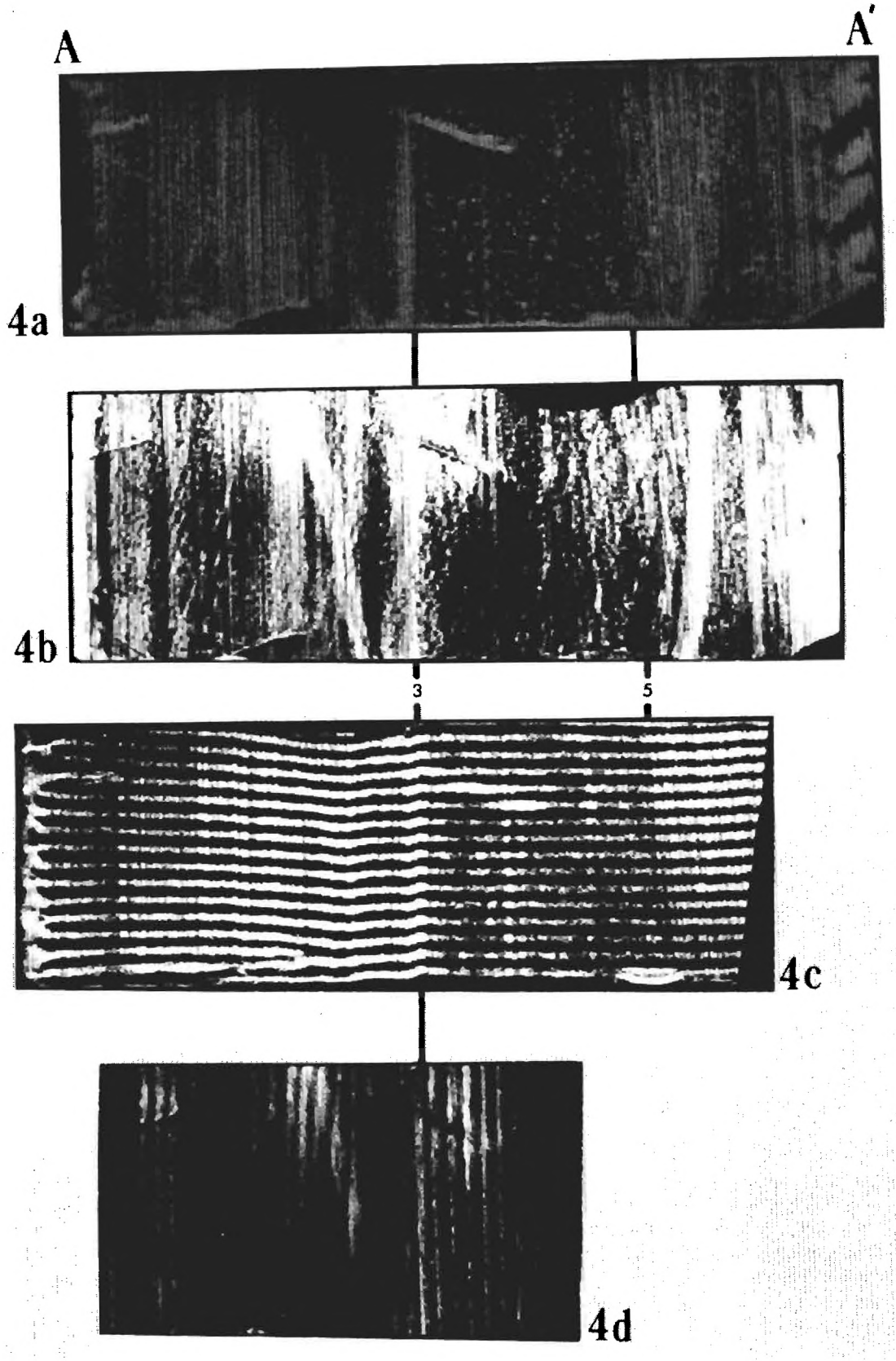
A
A'
4a
4b
3
5
4c
4d